This is a preprint, the final version is subject to change, of the American Mineralogist (MSA)
Cite as Authors (Year) Title. American Mineralogist, in press.
DOI: https://doi.org/10.2138/am-2018-6058

REVISION NO. 2

Eruption Triggering by Partial Crystallization of Mafic Enclaves at Chaos Crags, Lassen Volcanic Center, California

Melissa A. Scruggs[1] and Keith D. Putirka[2]

[1]Department of Earth Science, University of California Santa Barbara, 1006 Webb Hall, Santa Barbara, California, 93106-9630, melissascruggs@umail.ucsb.edu.

[2]Department of Earth and Environmental Sciences, California State University, Fresno, 2576 East San Ramon Avenue, M/S ST24, Fresno, CA 93740, kputirka@csufresno.edu.

Abstract

Magma mixing at arc volcanoes is common, but the manner in which mixing or mafic recharge may trigger volcanic eruptions is unclear. We test ideas of eruption triggering for the 1,103 ±13 y B.P. Chaos Crags eruption at the Lassen Volcanic Center, Northern California. We do so by applying mineral-melt and two-mineral equilibria from mafic enclaves and host lavas from six eruptive units of the Chaos Crags eruption to calculate crystallization conditions. Understanding that Chaos Crags are a type location for magma mixing, we estimate these P-T conditions by employing some apparently new methods to reconstruct pre-eruptive liquid compositions—which can be independently verified using various mineral-melt equilibria. We find that crystallization of "host" rhyodacite magmas occurs within the upper crust (at pressures of 0—1.7 kbar) over a ~300°C interval (temperatures ranging from 669—975°C) and that mafic magmas (which occur as enclaves within the host felsic samples) crystallized over a ~250°C

temperature interval (ranging from 757—1090°C), also within the upper crust, though extending to middle-crust depths (0—3.9 kbar). Notably, both host lavas and mafic enclaves contain crystals that are inherited from their opposing end-member, and both magma types contain plagioclase crystals that appear to have equilibrated with the resulting intermediate composition magmas; these intermediate composition plagioclase crystals indicate that some amount of time passed between both the recharge of magma into a felsic reservoir, and the mixing event that caused an exchange of crystals, before eruption.

We propose that mafic recharge – though it may have been the ultimate triggering event – did not immediately precede any of the eruptive events at the Chaos Crags. The most mafic (least mixed) enclaves in our collection are nearly aphyric, indicating that they were likely the first melts to enter the system, and quenched upon intrusion into a cold, upper crust felsic magma. Many high T Ol grains in enclaves also co-exist with Cpx, Pl and Amp crystals that crystallized from only slightly more evolved liquids, at temperatures that are low enough (e.g., 800-900^{o}C) to have possibly quenched earlier-formed, high-T Ol crystals, perhaps negating the use of Ol diffusion profiles as a record of mixing-to-eruption time scales (at the Chaos Crags, at least, they would only provide minimum times, which could be orders of magnitude less than actual times). And more crystalline enclaves record more mixing, and more cooling. It thus appears that recharge is required to reinvigorate an otherwise dormant Chaos Crags system, as described by Klemetti and Clynne (2014), but ~250^{o}C of cooling and crystallization, as recorded by many enclaves, provides the immediate cause of eruption—through increased magma overpressure by the exsolution of a fluid phase and increased buoyancy.

Keywords

magma mixing, eruption triggering, mafic enclaves, Chaos Crags, Lassen Volcanic Center

Introduction

Mafic recharge into the base of crustal magmatic reservoirs, and subsequent magma mixing, have both been widely implicated as a possible eruption trigger for arc volcanoes (Sparks et al. 1977, Huppert et al. 1982, Clynne 1999, Pallister et al. 1992, Kent et al. 2010; Cooper and Kent 2014). However, it is unclear which (if either) of these processes, recharge or mixing, are a proximate cause of eruption (see Putirka 2017). Petrologic evidence from numerous arc volcanoes indicates that a mixing event and eruption can occur concurrently (Woods and Cowan 2009), or that the time between mixing and eruption can range from days (Wallace and Carmichael 1994; Venezky and Rutherford 1997) or weeks (Huppert et al. 1982; Hammer and Rutherford 2003; Martin et al. 2008) to years (Huppert et al. 1982; Streck et al. 2002) or even decades (Costa and Chakraborty 2004) prior to eruption. Of course, in those cases where magma mixing is syn-eruptive, the mixing event is a result of - rather than a cause of - eruption. Another model for eruption triggering, sometimes referred to as second boiling (see Blake 1984; but also Daly 1911), involves increases in magmatic overpressure due to volatile saturation, exsolution, and accumulation of volatiles (primarily during crystallization of anhydrous phases).

By disentangling mixing end-members, we can estimate the P-T conditions of recharge and storage, and so better understand eruption triggering mechanisms. If a mafic recharge event were the proximate trigger of eruption, then crystals contained within mafic enclaves (Ol, Cpx, Pl) should largely record the *P-T* conditions under which the recharge magmas were stored prior to eruption (the middle or lower crust?). There should also be little time for magma mixing

(Petrelli et al. 2006; Petrelli et al. 2011), and the proportion of crystals derived from hybridized magmas should be small, if not absent (see Wallace and Carmichael 1994; Kent et al. 2010). On the other hand, if there were some delay between recharge and eruption, there may be time for recharge magmas to cool—the magnitude of the delay would then be a function of the degree of crystallization of recharge magmas (Folch and Martí 1998). In the case of a delay, there may also be time for mixing, and at least some re-equilibration of minerals that might precipitate from mixed liquids. If evolution of a fluid phase induced by extensive crystallization (Blake 1984) was the proximate eruption trigger, not only should mafic enclaves be replete with crystals that are precipitated at upper crustal pressures over a wide range of temperatures, but a considerable fraction of those crystals should derive from a range of intermediate magmas formed by varying degrees of mixing and crystallization (Coombs et al. 2000; Richer et al. 2004).

We test whether recharge is a proximate triggering mechanism for the 1,103 ±13 y BP eruption of Chaos Crags, by estimating the crystallization pressure (P) and temperature (T) conditions for crystals (olivine, Ol; plagioclase, Pl; clinopyroxene, Cpx; amphibole, Amp) found within mafic enclaves, which represent the rock record of recharge. The Chaos Crags eruptive products are useful, as they are characterized by the presence of mafic enclaves and are a well-known locality for the incomplete magma mixing processes that the enclaves represent (Wallace and Bergantz 2005). They are certainly representative of lavas produced by other recent eruptions of the LVC—for example, the majority of domes produced at other Eagle Peak sequence vents are characterized by similar mafic enclaves and disequilibrium mineral assemblages (Heiken and Eichelberger 1980; Clynne 1999; Feeley et al. 2008; Clynne and Muffler 2010). Mafic enclaves at Chaos Crags have been long-recognized to record magma mingling - the incomplete magma mixing of two end-member magmas (Heiken and Eichelberger

1980; Bacon 1986; Wallace and Bergantz 2005). . It has long been known that andesites and dacites, especially those at the Lassen Volcanic Center, are a product of magma mixing (Macdonald and Katsura 1965; Fountain 1979; Eichelberger 1974; Clynne 1999; Feeley et al. 2008) and as we detail below, we employ a new approach to such systems by using various and independent mineral-melt equilibria to estimate compositions of pre-mixing igneous liquids and *P-T* conditions of crystallization.

Geologic Setting

The Cascade Range of the northwestern United States is a continental volcanic arc overlying the Cascadia subduction zone, and extends from Mount Meager in southwestern British Columbia southwards to the Lassen Peak (Hildreth 2007). The Lassen area hosts distributed mafic volcanism and the Lassen Volcanic Center (LVC). LVC is a long-lived focus of volcanism comprising three phases of activity: 1) the Rockland caldera complex, a small caldera and dacite to rhyolite domefield (~825–609 ka); 2) Brokeoff Volcano, an andesitic stratocone (590–385 ka); and 3) the Lassen Domefield, a group of andesite to rhyodacite lava domes, flows and pyroclastic deposits (Clynne and Muffler, 2010). The youngest group of domes and flows - the still active Eagle Peak and Twin Lakes sequences - were emplaced beginning about 90 ka (Clynne and Muffler 2010). For a detailed background on the geologic setting of the Lassen region, the reader is referred to Guffanti et al. (1990), Blakely et al. (1997), Christiansen (2002), Clynne and Muffler (2010), Clynne et al. (2012), and Muffler and Clynne (2015).

Chaos Crags are the youngest eruptions within the Eagle Peak sequence, and are located in the Lassen Domefield just north of Lassen Peak (Christiansen et al. 2002). Chaos Crags

consist of six dacite to rhyodacite lava domes (Domes A-F, in order of decreasing age), and associated pyroclastic deposits (Fig. 1). The volume of erupted products is at least 1.2 km^3 (not including distal tephra; Clynne et al. 2012) and may be as much as ~2 km^3 (Heiken and Eichelberger 1980). The eruption began with emplacement of 2 pyroclastic flows followed by growth of Dome A, which plugged the vent. A large explosive eruption followed which mostly destroyed Dome A and produced a widespread pyroclastic flow, followed by theeruptions of Domes B–F. Chaos Crags eruptive units may be divided into two lithologically similar but subtly different groups: 1) the early pyroclastic flows and domes A and B (group 1), and 2) domes C through F (group 2) (Tepley et al. 1999; Wallace and Bergantz 2005). Radiocarbon ages indicate that the eruption began at 1,103 ±13 years BP (Clynne et al. 2008). The duration of the eruptive sequence is unknown, but unpublished paleomagnetic data suggest that the dome building eruptions lasted no more than a few decades after the explosive eruptions. (Clynne et al. 2008).

Methods

We present whole-rock elemental data for six host and 47 enclave samples (Appendix A), collected from each of Chaos Crags domes, A through F, and the upper pyroclastic flow, with accompanying mineral compositions for most samples (Appendices B-G). Enclaves were divided into cores and rims based on macroscopic differences in texture and color; where macroscopic differences were not evident, the outer 2 cm of the enclave was designated as the enclave rim. Cores and rims of enclaves were treated as separate samples for purposes of whole-rock geochemical analyses, to determine if compositional variations within individual enclaves were present.

Whole Rock Geochemical Compositions

Whole-rock geochemical compositions were determined using a Phillips Analytical Wavelength Dispersive X-Ray Fluorescence Spectrometer at California State University, Fresno. Care was taken to remove visually distinct disaggregated enclave fragments from host lavas prior to analyses, however, as some individual crystals in felsic host materials are enclave-derived, a perfect separation of enclave and host is not possible. Sample powders were ground for 3-5 minutes in a tungsten carbide shatterbox; mafic enclave powders were calcined for 10 minutes at 1000°C, and host powders calcined for 10 minutes at 900°C to ensure dehydration of sample and oxidation of Fe^{2+} to Fe^{3+}. Analysis of major oxide components was conducted using the fused glass bead method (Busby et al. 2008). Relative errors (%RSD) for USGS calibration standards are: BCR-2: 0.55% SiO_2, 0.89% TiO_2, 0.67% Al_2O_3, 0.36% Fe_2O_3, 0.28% MgO, 0.28% CaO, 0.01% Na_2O, 0.56% K_2O, and 0.01% P_2O_5; GSP-2: 0.15% SiO_2, 1.5% TiO_2, 0.01% Al_2O_3, 0.20% Fe_2O_3, 4.1% MgO, 0.94% CaO, 2.13% Na_2O, 0.37% K_2O, and 0.01% P_2O_5 (Putirka et al. 2014).

Mineral Compositions

Mineral compositions for plagioclase (Pl), clinopyroxene (Cpx), orthopyroxene (Opx), olivine (Ol), amphibole (Amp), magnetite (Mag), and ilmenite (Il) were obtained at the University of California, Davis using a Cameca SX-100 electron microprobe and at the U.S. Geological Survey (USGS) Menlo Park using a JEOL JXA-8900 electron microprobe; specific parameters for analyses of individual mineral phases are given in Table 1. X-ray intensities were converted to wt.% concentrations using automated CITZAF matrix corrections (Armstrong 1995). Polished thin sections were coated with an ~25 nm layer of C prior to analysis (Watson 1955).

Reconstructing Liquid Compositions—the Need and Approach

At least since Green's (1975) study of komatiites, we have understood that mineral compositions provide a powerful means to delimit the compositions of mafic silicate melts, whose compositions may be veiled by mixing or differentiation, but whose identity is crucial to understanding mantle processes. The need for reconstructing liquid compositions stems from (a) a long-standing recognition that mafic magmas are a slurry of not-necessarily-equilibrated Ol crystals, and liquids (e.g., MacDonald 1944; Murata and Richter 1966), as well as supercritical fluids and possibly, exsolved volatiles (Spera 2000; Lesher and Spera 2015), and (b) that so-called primary magmas (undifferentiated mantle partial melts) are rarely, if ever, erupted directly to the surface (e.g., O'Hara 1968; Stolper 1980). Mineral compositions are an invaluable tool for liquid composition reconstruction, as they are capable of carrying a record of liquids that are otherwise lost to mixing and/or differentiation. We thus reconstruct mafic parent magma compositions (e.g., Herzberg and O'Hara; Putirka 2016b) to estimate the P-T conditions of crystallization and to better understand the mineralogy and composition of the Chaos Crags system.

To date, however, liquid reconstruction methods have not been applied to arc-related andesites and dacites—despite an equally long-standing recognition that magma mixing is nearly ubiquitous in arc settings (MacDonald and Katsura 1965; Eichelberger 1975). Knowledge of intermediate liquids, though, is no less important, for estimating P-T conditions of magma recharge, storage, and mixing, which in turn reveal how volcanic eruptions are triggered (Putirka 2017). The Chaos Crags are a near-perfect target for such an attempt as they represent something of an archetype of magma mixing (Heiken and Eichelberger 1980; Tepley et al. 1999). They

contain abundant and sometimes nearly aphyric mafic enclaves, which provide an uncomplicated view of mafic end-member liquids. Furthermore, experiments by Quinn (2014) yield information of felsic liquid end-members, and numerous whole rock compositions (e.g., Heiken and Eichelberger 1980; Tepley et al. 1999; this study) tell us about what lies between. Perhaps petrologists have been dissuaded from the attempt due to the mineralogic complexity of intermediate magmas—but herein lies the advantage: a panoply of minerals with well-calibrated tests of equilibrium (e.g., Ol: Roeder and Emslie 1970; Cpx: Putirka 1999; Pl: Putirka 2005: Amp: Ridolfi and Renzulli 2011, Putirka 2016a) offers multiple, independent tests of liquid compositions so that igneous liquids can be even better constrained than their mineralogically more simple mafic counterparts.

Our methods of liquid reconstruction vary depending upon the mineral phase in question (see below for details), but our general approach is as follows: (1) We select a candidate liquid among multiple, nearly aphyric compositions, that has the correct Fe/Mg (using T- and P-independent models, Putirka 2016b) to explain many observed Ol and Cpx crystals found within Chaos Crags enclaves (Roeder and Emslie 1970; Putirka 2016a), or the correct SiO_2 to explain observed high-An Pl, or low-Si Amp (Putirka 2005; 2016b). (2) From such a liquid, we then estimate an equilibration temperature (*T*) and, additionally for Cpx, a pressure (*P*) using the models of Putirka (2005, 2008, 2016a, b). (3) We input the calculated liquid composition and estimated *P*-*T* conditions into the (*T*- and *P*-sensitive) models of Putirka (1999, 2005) to predict Ol, Cpx or Pl components (re-calculating Fe-Mg exchange), comparing these to observed phase compositions and model error. (4) We then compare the *T* estimates from the various mineral-liquid equilibria, ensuring that any differences are consistent with experimentally-determined phase equilibria (see below for details). (5) If the hypothetical liquid fails to predict observed

mineral compositions in steps (3)-(4), we adjust the liquid by either (i) adding or subtracting observed mineral phases (as if moving along a liquid line of descent) or (ii) adding/subtracting a felsic Chaos Crags whole rock composition (as if moving along a crystal + liquid mixing trend) or (iii) adding a glass composition from Quinn (2014) (as if mixing liquids only), until the tests of step (1) are satisfied, where we repeat the process moving to step (2) to calculate *T* and *P*, etc. To anticipate some of our results, we obtain very similar, if not identical, mafic liquid compositions, and *T* estimates from independent calculations involving Cpx, high-Fo Ol, high-An Pl and low-Si Amp, and similar felsic liquid compositions from high-Si Amp, low-Fo Ol and low-An Pl.

Our tests of equilibrium are effectively a calibration of phase boundaries as they may vary with P-T and compositional variables. As such, we conduct something of a redundancy check, where in (4), we examine crystallization order and *T* contrasts with experimental phase relations based on hydrous arc bulk compositions (Fig. 2; Baker and Eggler 1983; Rutherford et al. 1985; Housh and Luhr 1991; Gaetani et al. 1994; Grove et al. 1997; Moore and Carmichael 1998; Scaillet and Evans 1999; Blatter and Carmichael 2001; Hammer et al. 2002; Grove et al. 2003; Holtz et al. 2005; DiCarlo et al. 2006; Rader and Larsen 2013; Quinn 2014; Waters et al. 2015); these tests are confirmed by Rhyolite-MELTS (e.g., Ghiroso and Sack 1995; Gualda et al. 2012), but since estimates of error are not provided for predicted values of *T*, *P* or phase composition, this model's usefulness is limited. As a final test, we check whether our hypothetical liquids either (a) fall on existing Chaos Crags whole rock trends (whole rocks are 0-50% crystalline, so are mostly liquid), or (b) lie on an extension of such trends so as to act as an end-member to a magma mixing or fractional crystallization process.

We caution that our approach is not foolproof. Within error of our equilibrium tests, some observed crystals can form from different liquids. For example, liquids with quite different SiO_2 or Al_2O_3 might have the correct Fe/Mg ratio to explain high Fo Ol. We also cannot guarantee that all minerals within Chaos Crags lavas are a product of equilibrium crystallization, nor that such minerals precipitated directly from Chaos Crags liquids (as opposed to minerals culled from the crystalline mush underlying the LVC; see Klemetti and Clynne 2014, and Schrecengost et al. 2016). However, several items mitigate against these potential pitfalls. For example, many of our calculated (and observed) mafic liquids are saturated in Pl, a well as Ol, which then highly restricts possible SiO_2 and Al_2O_3 contents (and other oxides); and for liquids where Ol is the only apparent saturating phase, only a small range of liquid compositions can explain Chaos Crags whole rock trends. Second, Chaos Crags are comprised of six different domes, each providing an independent test of the Chaos Crags system. Mineral populations at these six domes are highly repeatable, and the equilibrium tests are convergent, making it quite unlikely that our calculated liquids or P-T results are grossly affected by xenocrysts or disequilibrium processes.

"Parental" Liquid Compositions, fO_2 and H_2O Contents. We start out tests of equilibrium with mafic inclusions that contain <1% phenocrysts, as their bulk compositions are effectively liquids (Table 2). These enclaves (a) tend to be similar in composition (See Appendix A), (b) are among the most mafic enclaves observed at Chaos Crags (4.5-5 wt.% MgO), and (c) almost always contain Pl + Ol ± Cpx. For modeling purposes (Table 3), we use sample CC-A-I-6 (<1% crystals; 4.98 wt.% MgO; 53.2 wt.% SiO_2). We find that some minerals are indeed in equilibrium with such a liquid (olivine, clinopyroxene and high-An plagioclase), but most are not. To obtain an equilibrium liquid composition, we explore a range of mafic and felsic magma compositions by mixing CC-A-I-6 with various Chaos Crags whole rock compositions, or

rhyolitic glass compositions obtained from phase equilibria experiments (Quinn 2014) on Chaos Crags host lavas, until (a) mineral-melt equilibrium tests are satisfied and (b) the calculated liquid falls on Chaos Crags whole rock composition trends. The Results section and Table 3 notes the suite of liquids that are required to explain the panoply of mineral and whole rock composition variations.

Eventually, we wish to use our calculated equilibrium liquids to estimate *T*, and such estimates are significantly affected by assumed water contents. Fortunately, Collins et al. (2012) and Quinn (2014) provide measurements of such, from melt inclusions of minerals present in Chaos Crags eruptive products. They obtain estimates of H_2O = 4 wt.% for mafic enclaves and H_2O = 5.6 wt.% for felsic host magmas. Given this narrow range of water contents, we interpolate using:

$$H_2O\ (wt.\%) = 0.383 + 0.06955[SiO_2\ wt.\%] \quad (1)$$

This equation is only valid at the Chaos Crags, and has an error that is not clear, but probably close to the difference between the two water measurements (1.6 wt.%). Oxygen fugacity (fO_2) strictly has no effect on any of the models used here: we apply models (Putirka 2008, 2016a, b) that are calibrated using experiments performed over a very wide range of fO_2, and that assume all Fe is FeO. It is essential that any model is applied precisely as calibrated, otherwise systematic error would be introduced (so it is essential, for example, not to "correct" for fO_2 variations, and so remove Fe^{3+} that was never removed during calibration). Any errors resulting from natural ranges in fO_2 are included in published model error estimates, including our use of Fe-Mg exchange equilibria, which are conducted using fO_2-independent models from Putirka (2008; 2016a, Eqn. 8a; 2016b). In our Results section, we will show evidence that fO_2 at Chaos

Crags was ~1.5 log units above the Ni-NiO buffer—well within the range of experimental fO_2 conditions of the various model calibrations.

Clinopyroxene-equilibrated Liquids. We calculate Chaos Crags magma compositions that precipitate clinopyroxene by using two tests of equilibrium. We first apply a Fe-Mg exchange equilibrium constant, $K_D^{Fe\text{-}Mg}$ = 0.27 ±0.03 (where $K_D^{Fe\text{-}Mg}$ = ($[X_{FeO}^{Ol}]/[X_{MgO}^{Ol}]$)/($[X_{FeOt}^{liq}]/[X_{MgO}^{liq}]$), and FeO_{tot} = total Fe as FeO), and either accept a bulk host composition as a liquid if it has low crystallinity and falls within 1σ error, i.e., $K_D^{Fe\text{-}Mg}$ = 0.24-0.31, or we add a Chaos Crags rhyodacite magma to CC-A-I-6 until the calculated liquid reaches $K_D^{Fe\text{-}Mg}$ = 0.27 (see Deposit Item 1). We then calculate *T* and *P* using the H_2O-dependent thermometer (Putirka 2008; Eqn. 33), using estimates of H_2O^{liq} from Eqn. 1. Pressure is then calculated using a new barometer from Neave and Putirka (2017). We then apply equilibrium tests (Putirka 1999; Eqns. 2.1 and 2.2) to predict diopside + hedenbergite (DiHd) and enstatite + ferrosilite (EnFs) components in clinopyroxene. We accept as viable all those liquids (and *P*-*T* conditions) where (a) the predicted values of DiHd and EnFs fall within a 1σ error bounds (Putirka 1999) of observed values and (b) the calculated liquids fall on observed Chaos Crags whole rock trends (Fig. 3) (see Deposit Item 2).

Olivine-equilibrated Liquids. For olivine, we use the fO_2- and composition-independent $K_D^{Fe\text{-}Mg}$ (Putirka 2016; Eqn. 8a; Deposit Item 3), adding to CC-A-I-6 a range of different hypothetical magma compositions (see Results) until $K_D^{Fe\text{-}Mg}$ = 0.30. We then apply Eqn. 2 of Putirka et al. (2007) and H_2O contents from Eqn. (1) to obtain *T*, assuming *P* = 2 kbar (from clinopyroxene and amphibole; see Results). Most olivine grains have compositions that are quite close to equilibrium with CC-A-I-6, requiring just 10% or less of a more evolved or more primitive magma to reach equilibrium. But, for olivine grains at $Fo_{69\text{-}77}$ (a small but ubiquitous

298 subset), we must introduce some of our results to explain our methods. At least three Chaos
299 Crags compositions have sufficiently low Mg# to explain olivine grains with <Fo_{77} (Fig. 3a): (a)
300 rhyolites (SiO_2 >70 wt.%), (b) high K_2O andesites (SiO_2 = 55-61 wt.%) and (c) low MgO
301 basaltic-andesites (SiO_2 = 52-55 wt.%). Lacking observable or experimental evidence for Chaos
302 Crags rhyodacites reaching olivine saturation, we reject (a) as a viable option and rely on (b) and
303 (c) as possible end-member compositions for olivine crystals with compositions <Fo_{77}. We thus
304 first add a Chaos Crags rhyodacite to CC-A-I-6 (rhyodacite being the most abundant low-Mg#
305 material, small amounts of which explains small variations in Fo content in many of our
306 enclaves) to reach $K_D^{Fe\text{-}Mg}$ = 0.30; if SiO_2^{liq} <61 wt.% we accept the result; if SiO_2^{liq} >61 wt.%,
307 we instead add a high K_2O andesite to CC-A-I-6 (this andesite being the next most abundant
308 low-Mg# composition). If this calculated liquid also has SiO_2^{liq} >61 wt.% we instead add a low
309 MgO basaltic andesite, and in this last case, we only accept the liquid if it has SiO_2^{liq} ≤55 wt.%,
310 this being the maximum SiO_2^{liq} for such andesites at Chaos Crags. This process finds a viable
311 liquid for effectively all our olivine analyses (none failing the final test) (Fig. 3). Clearly, we do
312 not obtain a unique solution for each individual olivine. But as noted above, most of these
313 calculated liquids can also be shown to be suitable for equilibration with other observed mineral
314 compositions and can explain Chaos Crags bulk compositions.

315 **Amphibole-equilibrated liquids.** For amphibole, we use Eqn. 10 of Putirka (2016b),
316 which allows one to estimate an equilibrium value SiO_2^{liq} (to a 1σ of ±3.6 wt. %), using a
317 measured amphibole composition as input. For each amphibole composition, we add rhyodacite
318 to CC-A-I-6 until the equilibrium SiO_2^{liq} is obtained. We then accept as viable those liquids (Fig.
319 3) that fulfill all three of the following conditions: (a) the calculated liquids fall within a 2σ range
320 of the expected Fe-Mg exchange equilibrium value of 0.28 (Putirka 2016b; Eqn. 2; Deposit Item

4); (b) *P*-estimates from Eqns. 7a and 7b from Putirka (2016b) agree within 3 kbar; (c) *T* estimates from Eqns. 4a and 4b of Putirka (2016b) agree within 50°C. Also, for individual amphibole that satisfy the key filters from Anderson and Smith (1995) (Fe#<65; *T*<850°C; see Putirka 2016b) we apply the Anderson and Smith (1995) Al-in-hornblende barometer and the amphibole-only thermometers of Putirka (2016b). These are highly restrictive tests, but effectively eliminate both strongly negative *P* estimates, and *P* estimates that exceed those obtained from clinopyroxene (we deem it highly unlikely that amphibole saturation occurs at a higher *P*, and yet much lower *T* than clinopyroxene).

Plagioclase-equilibrated liquids. To calculate plagioclase-equilibrated liquids, our method is to add a Chaos Crags rhyodacite to CC-A-I-6, calculating *T* at each step (assuming *P* = 2 kbar and water contents from Eqn. 1 above), using an average *T* from Eqns. 22 and 23 from Putirka (2008). We use that average *T*, and the resulting liquid, to predict the An content that should precipitate from such a liquid (at the assumed/calculated *P*-*T* conditions) using Eqn. (E) of Putirka (2005). We then apply two new tests: non-tholeiitic plagioclase saturated experimental liquids (from LEPR; Hirschmann et al. 2008) exhibit a distinct linear relationship between the An content of plagioclase and both SiO_2^{liq} and CaO^{liq}, from which we obtain

$$SiO_2^{liq} = 87.1 - 0.38[An] \quad (2)$$

$$CaO^{liq} = \exp(-1.0 + 0.0377[An]) \quad (3)$$

where [An] is the % value for the anorthite content of plagioclase, and oxides are in weight %. These equations predict SiO_2^{liq} to ± 3.9 wt.% and CaO^{liq} to ±1.2 wt.%; the experiments used for calibration have H_2O(wt.%) = 0.6–12, *T* = 700–1250°C and *P* = 0.4–22 kbar, and so allow a further test for viable equilibrium liquids, independent of estimates of *P*, *T*, or H_2O. For each plagioclase composition, we calculate a liquid, using our mixing end-members, so that measured

and predicted An contents (Putirka 2005; Eqn. E) match precisely. We accept those calculated liquids as being viable, if (a) the calculated values for SiO_2^{liq} and CaO^{liq} are within 2σ error of the values expected using Eqns. (2) and (3), and (b) the liquids also fall on Chaos Crags whole rock composition trends, or their extension (see Deposit Item 5).

Oxides. Compositions of touching magnetite-ilmenite pairs were used to determine pre-eruption equilibrium conditions of host lavas and mafic enclaves. Although it is reasonable to assume that touching oxide pairs have equilibrated (Bacon and Hirschmann 1988), this is not the case for oxides which have undergone re-equilibration due to slow cooling after crystallization (Hammond and Taylor 1982), or for those oxides which have oxidized and exsolved (Bacon and Hirschmann 1988). We therefore apply the $(Mg/Mn)^{mt\text{-}il}$ test of Bacon and Hirschmann (1988) to confirm equilibration of measured two-oxide pairs in this study (Deposit Item 6). We recalculated wt.% FeO and wt.% Fe_2O_3 within Fe-Ti oxides using the method of Carmichael (1967) as employed by ILMAT software (Lepage 2003).

Estimates of Crystallization Temperatures, Pressures, fO_2, and H_2O Contents

Mineral-melt equilibria geothermometers and geobarometers of Putirka (2005, 2008, 2016), the two-pyroxene Fe-Mg exchange equilibria thermobarometer of Putirka (2008), the amphibole-only thermometer of Putirka (2016), and the mineral Fe-Ti exchange equilibria thermobarometer of Ghiorso and Evans (2008) were used to place constraints on pre-eruptive *P-T* and fO_2 conditions of eruptive products. For the small subset of those Cpx grains for which we could not obtain a satisfactory liquid composition using the methods noted above, we then tested such Cpx grains for possible equilibrium with Opx—in this case using only those Opx grains that occur in the same mafic enclave sample. To test for equilibrium with Opx, we apply a Rhodes diagram test using $K_D(Fe\text{-}Mg)^{cpx\text{-}opx} = 1.09 \pm 0.14$ (see Putirka 2008; Deposit Item 7) and report

only those P-T conditions from two-pyroxene pairs that fall within 2σ error bounds for presumed equilibrium (Putirka 2008).

Results

The below results describe only those samples examined in this study (Appendix A), and do not reflect those samples which have already been described in earlier studies (e.g., Tepley et al. 1999 and Underwood et al. 2012), or those samples which currently reside in unpublished databases.

Mineral Textures

Lithologic and petrographic descriptions of Chaos Crags lavas are given in Christiansen et al. (2002). These lavas are porphyritic hornblende-biotite dacites to rhyodacites (referred to herein as rhyodacites to maintain terminology consistent with that of Christiansen et al. 2002), characterized by a predominantly disequilibrium phenocryst assemblage, and abundant mafic enclaves (Heiken and Eichelberger 1980; Tepley et al. 1999). In addition to visually distinct mafic enclaves, host lavas also contain enclave fragments and individual crystals interpreted to be the product of enclave disaggregation, the abundance of which increases over the eruption sequence (Tepley et al. 1999, Underwood et al. 2005).

Our work confirms what has already been described in prior studies, and the summary by Tepley et al. (1999) is quite appropriate to the description of our samples. It is perhaps worth re-emphasizing that Ol, Cpx and high-An Pl (An>80) are found almost exclusively in mafic enclaves, and are mostly absent from host rhyodacite samples, while quartz and low-An Pl (An<40) are found mostly in host rhyodacite samples, but still occur in mafic enclaves, indicating that during magma interaction, the degree of hybridization (Petrelli et al. 2006)

between the two magmas was anything but uniform. As alluded to above, we also find that many mafic enclaves, especially those with the highest MgO contents (3.5-5 wt. %) are nearly aphyric, containing <2% crystalline material. And so despite the prevalence of mixing, it is possible to identify at least some of the mafic liquids that are the parents to mafic crystalline phases. However, we did not discover significant compositional contrasts between phenocrysts, microphenocrysts and groundmass crystals of the same mineral species, and for this reason we did not pursue more detailed comparison of mineral textures and composition. Additionally, because we were interested in obtaining *P-T* estimates of crystalline phases from models that assume equilibrium between a crystal and liquid, we avoided clearly disequilibrium textures, such as zones of spongy plagioclase or dendritic or needle-like phases, etc. Many of our crystals are indeed rounded or reversely zoned, and in these cases we analyzed core and rim compositions in the hope of reconstructing pre- and post-mixing liquid compositions (so a core or rim composition is unlikely to have crystallized from its whole rock host, but it must have crystallized from some sort of liquid—whose composition it is is our aim to reconstruct). We also note that mixing is not necessarily a temporally singular process; rather it can be recurring and continual, and it is reasonable to expect a range and distribution of liquids to be generated that might not be much different than the whole rocks (which are comprised of a mixture of such liquids, and their various mineral assemblages). This is not to say that further exploration of mineral textures would not be valuable: if composition can be linked to crystal morphology petrologists might obtain a powerful shortcut to estimating conditions of crystallization, with possible links to crystal nucleation and growth. But our main goal here is to present a new analysis of an arc system, where for the first time, liquid compositions are reconstructed in detail from observed mineral phases, and the *P-T* conditions of their genesis are determined.

Geochemical Compositions of Eruptive Products

Chaos Crags lavas are dacitic to rhyodacitic, characterized by the presence of basaltic-andesitic mafic enclaves and subtle temporal changes in composition of both enclave and host materials (Appendix A). Total alkali-silica (TAS) contents (LeBas 1986) show that whole-rock compositions are basaltic-andesite (enclaves), andesite (enclaves) and dacite to rhyodacite (felsic host for enclaves) (Deposit Item 5).

Chaos Crags pyroclastic flows and lavas have dominantly rhyodacitic (67.5 to 71 wt.% SiO_2) bulk compositions (Appendix A). The compositions fall into 2 homogeneous groups: 1) early pyroclastic flows and domes (or Group 1), and 2) domes C–F (or Group 2). Four analyses of Group 1 units contain an average of 69.40 wt.% SiO_2, and four analyses of Group 2 units contain an average of 67.83 wt.% SiO_2. Thus, on average the Group 1 units contain about 1.6 wt.% higher SiO_2 than the Group 2 units.

Bulk compositions of the basaltic andesite to andesite mafic enclaves range from 51.88 to 60.44 wt.% SiO_2. As before, the compositions fall into two relatively homogeneous groups, enclaves from the early pyroclastic flows and domes (or Group 1), and 2) enclaves from domes C–F (or Group 2). Thirty analyses of enclaves from Group 1 units contain an average of 55.2 wt.% SiO_2, and 58 analyses of Group 2 units contain an average of 57.0 wt.% SiO_2. The difference between the host and enclave compositions becomes more narrow throughout the eruption sequence (Fig. 4), as enclaves become more felsic and host lavas become more mafic, from the earliest Dome A to the youngest Dome F; on average Group 1 units contain abo ut 1.6 wt.% lower SiO_2 than Group 2 units, and the difference between the average host and average enclave composition is about 14 wt.% in Group 1 and about 11 wt.% SiO_2 in Group 2. These values are probably closely representative of the enclave population as a whole, and are similar

436 to compositional differences between Chaos Crags host and enclave compositions as presented
437 by Heiken and Eichelberger (1980), Tepley et al. (1999), and Clynne and Muffler (2010).

438 The majority of mafic enclaves do not exhibit core-to-rim compositional contrasts that
439 fall outside of analytical uncertainty. However, five of the mafic enclaves analyzed exhibit
440 distinct variations in major oxides (Deposit Item 8). Enclave rims generally have the greatest
441 wt.% SiO_2, and the least wt.% MgO and Al_2O_3, except for enclave CC-E-I-10, which exhibits a
442 4.05 wt.% decrease in SiO_2 from enclave core to rim. As noted above, we use unzoned, aphyric
443 enclave compositions as a mafic end-member liquid for explaining Chaos Crag mineral
444 compositions and estimating crystallization P-T conditions.

445 **Textural Features of Mafic Enclaves**

446 Mafic enclaves of Chaos Crags exhibit a variety of textures, including aphanitic,
447 porphyritic with aphanitic groundmass, porphyritic with fine-grained phaneritic groundmass, and
448 fine-grained phaneritic [see Heiken and Eichelberger (1980), Tepley et al. (1999), Hootman
449 (2011), and Schmidt (2014) for additional textural descriptions of Chaos Crags mafic enclaves].
450 Enclave groundmass textures also vary within any given dome, and even within an individual
451 enclave. Enclaves may exhibit crenulated margins and quenched rims, but not all enclaves have
452 retained their quenched or crenulated margins (Deposit Item 9). Excluding groundmass phases,
453 total crystallinity in the mafic enclave samples varies from <1 % to ~20% (Table 2).

454 Mafic enclaves measured in this study have diameters ranging from <4 cm to over 50 cm;
455 enclave fragments of <4 cm in diameter are interpreted to be the product of enclave
456 disaggregation. Despite the textural and compositional variety of mafic enclaves found within
457 the Crags' eruptive products, no correlations were found between groundmass texture and
458 temperature, pressure, or whole-rock geochemistry.

Disequilibrium Mineral Assemblage

Chaos Crags eruptive products—both enclaves and host lavas—contain many mineral phases that are not at equilibrium with either each other, or their respective bulk rock composition (see Tepley et al. 1999 and Underwood et al. 2012).

Oxides. Host lavas in domes A-E contain both titanomagnetite and ilmenite; dome F host lavas contain only titanomagnetite (Appendix B; Deposit Item 10). Mafic enclaves generally contain either solely titanomagnetite or, rarely, only ilmenite as the oxide species. The outermost rim of enclave CC-B-I-9 contains touching pairs of titanomagnetite and ilmenite, located within host-derived material that has been incorporated into the rim of the enclave.

Pyroxene. Clinopyroxene and orthopyroxene are present almost solely within Chaos Crags mafic enclaves, although a few rare crystals of both occur in rhyodacitic host lavas (Appendices C and D; Fig. 5). Pyroxenes present within mafic enclaves occur as fresh to variably reacted phenocrysts, reaction rims surrounding quartz and/or olivine, as pseudomorphic replacement products, and as groundmass crystals (Fig. 6).

Olivine. Olivine is present in most of the analyzed mafic enclaves, but like pyroxene is mostly absent from host lavas. Olivine occurs as variably reacted euhedral to subhedral phenocrysts or as groundmass crystals within mafic enclaves, and a few stray highly-reacted olivine crystals were present within host lavas; olivine phenocrysts are rare within all eruptive products in the latter half of the eruptive sequence (Fig. 6). Forsterite contents range from Fo_{69} to Fo_{83} (Appendix E; Fig. 7).

Amphibole. Amphibole is abundant in Chaos Crags host lavas as large (up to 4 mm) phenocrysts, and is found in many mafic enclaves as variably-reacted euhedral to subhedral phenocrysts, acicular microphenocrysts, fine-grained groundmass, and glomeroporphyritic clots

accompanied by biotite and Fe-Ti oxides (Fig. 6). Host lavas contain magnesiohornblende, while amphibole compositions present within mafic enclaves range into the actinolite and tschermakite fields in a Mg# vs. Si diagram (Appendix F; Fig. 8).

Plagioclase. Plagioclase is dominant crystalline phase within Chaos Crags host and enclave materials, and occurs as phenocrysts, microphenocrysts, and as groundmass (Fig. 6). Plagioclase within mafic enclaves and host lavas range from An_{23}-An_{93}, with An_{23}-An_{27} compositions restricted to the cores of large, highly-reacted phenocrysts (Appendix G; Fig. 9).

Reconstruction of Liquid Compositions

Mafic Parental Liquids at the Chaos Crags. We find our low crystallinity mafic inclusion CC-A-I-6 works remarkably well as a parent magma for many olivine, clinopyroxene, and plagioclase crystals found in Chaos Crags mafic enclaves (regardless of the bulk composition of the mafic enclave host). Sixty percent (n=360) of our measured olivine require ≤10% addition of a more mafic magma (Table 3) to reach Fe-Mg exchange equilibrium, apparently precipitating from a liquid with an average of 5.5 wt.% MgO (compared to the maximum 5 wt.% MgO of our typical aphyric mafic enclaves). Our highest Fo olivine (Fo_{82}) and highest An plagioclase ($An_{90\text{-}92}$) both indicate equilibration with a Lassen magma that is more mafic (6.0-6.7 % MgO) than observed among Chaos Crags mafic enclave samples (Fig. 3; Table 3). To model this magma, we use sample LC84-650A (Earthchem) from the 27 ka Lassen Peak eruption (53.2 wt.% SiO_2; 10.1 wt.% MgO; Table 3) as a mixing end-member. This sample, LC84-650A (Earthchem) is not aphyric, and we do not have data to test whether its Cpx and Ol grains are in equilibrium with the whole rock; but we need not assume that it is a liquid—only that it falls on a liquid+crystal mixing trajectory that is appropriate for explaining Chaos Crags mineral and liquid compositions. By contrast, our highest *T* clinopyroxene do not require

anything near such a mafic end-member, as they appear to have instead equilibrated with liquids having 4-5 wt.% MgO—derived mostly by mixing CC-A-I-6 with small amounts (<15%) of rhyodacite magma (Fig. 3). These results are consistent with petrographic observations of Chaos Crags enclaves where (a) phenocryst phases are dominantly Ol + Pl ± Cpx, and (b) clinopyroxene is greatly subordinate in abundance to olivine and plagioclase. We thus infer that 1) the recharge magmas that entered the Chaos Crags eruptive reservoir contained up to 6.7% MgO prior to interaction with felsic materials, and were saturated with Ol + Pl ± Cpx; and 2) most clinopyroxene saturation occurred following contact of recharge magmas with resident felsic materials.

Intermediate and Evolved Chaos Crags Liquids. Except for olivine, the vast majority of observed mineral compositions (>90%) can be explained by mixing CC-A-I-6 with either rhyolitic liquids from Quinn (2014) or a Chaos Crags rhyodacite (sample CC-D-H-1; 68.04 wt.% SiO_2; 3.49 wt.% FeOt; 1.62 wt.% MgO; 2.58 wt.% K_2O), and for all our mafic phases, it matters little which composition is used as the resulting *P-T* estimates are indistinguishable (within 0.1^o C and 0.01 kbar). The reason that the choice of felsic end-member matters so little is because Chaos Crags whole rock trends are linear, and so the trajectories of various bulk compositions are effectively equivalent (until one attempts to model highly felsic liquids, as we show below). Since we assume that mafic recharge magmas interacted with a bulk rock that was partially crystalline and dacitic, rather than the rhyolitic melts that would occur in the matrix of such a rhyodacite, all our calculations for our mafic phases use the CC-D-H-1 as a mixing end-member. A few olivine crystals have low Fo (Fo_{69-77}), and so require a relatively low Mg# liquid (Fig. 3). These lower Fo-content crystals would appear to record an evolved liquid. The key question is of what type? Along the mixing trend already noted, involving CC-D-H-1, only a rhyolitic liquid

would have the requisite Fe/Mg ratios to explain Fo_{69} olivine crystals. But the experiments of Quinn (2014) do not indicate that felsic Chaos Crags liquid reached olivine saturation. We can instead explain low Fo_{69-77} grains using a high K_2O andesite (CC-E-I-13 Rim, 59.49 wt.% SiO_2; or LC84-634, 61.39 wt.% SiO_2), or a high FeO, low MgO basaltic-andesite (S-D-4, 54.61 wt.% SiO_2); these Ol-saturated liquids have 2-5.5 wt.% MgO and 53-61 wt.% SiO_2 (Fig. 3). We thus conclude that all our olivine grains are derived from basaltic to andesitic liquids, but our results do not indicate how these particular liquids (along the CC-E-I-13 or LC84-634 trends) are created—these end members may represent highly unusual liquid lines of descent or products of wall rock assimilation.

In contrast, the continuum of plagioclase compositions requires a much wider range of liquid compositions, covering the entire span of observed Chaos Crags whole rocks, and ranging to as felsic as 79.1 wt.% SiO_2 (Fig. 3). We also require a liquid with 6.1 wt.% MgO, 19.3 wt.% Al_2O_3, 52.8 wt.% SiO_2, and 10.3 wt.% CaO to yield the highest An_{92} plagioclase compositions (Fig. 3). This composition is quite similar to that needed to precipitate Fo_{82} olivine, except for having greater Al_2O_3 than the liquid derived by projecting Mg# towards the Lassen Peak mafic composition (LC84-650A; Earthchem). However, our An_{92}-saturated liquid also has an Mg# that yields Fo_{82} olivine, so the primitive recharge liquids feeding the Chaos Crags system might not be identical to those that energized the earlier Lassen Peak (27 ka) eruptive episode.

P-T Conditions of Chaos Crags Recharge and Felsic Magmas

Oxides. Nominally equilibrated Fe-Ti two-oxide pairs obtained from host lavas in this study yield equilibration conditions of 669°C—764°C ±51°C and fO_2 at +1.43—1.76 log units above the Ni-NiO buffer. Within the only mafic enclave in which they are present, two-oxide pairs yield equilibration conditions of 757°C—821°C ±51°C and fO_2 at +1.24—1.37 log units

above the Ni-NiO buffer (Fig. 10). We suspect that the low-T ends of these ranges are pre-mixing storage conditions (Klemetti and Clynne 2014; Cooper and Kent 2014), not eruption conditions as Quinn (2014) obtains 760-775°C for Fe-Ti oxides, at NNO + 1.35.

Pyroxene. Within mafic enclaves, a subset of coexisting orthopyroxene-clinopyroxene pairs that pass equilibrium tests (and fail to pass our tests of cpx + liq equilbirum) yield crystallization temperatures of 903—1022 ±56°C and pressure estimates of crystallization ranging from 0—4.4 ±3.2 kbar (Fig. 11). It should be cautioned that these estimates may be more uncertain than the error values indicate, since we cannot be certain that these phases have not been accidentally thrown together during mixing, and we only have the Fe-Mg exchange tests of Putirka (2008) to test for equilibrium.

For clinopyroxene-liquid equilibria we find that most Cpx grains precipitated from magmas very similar to our observed enclave whole rock compositions (with <55% SiO_2; Fig. 3), but a few are consistent with precipitation from intermediate composition liquids, ranging up to 62-63% SiO_2 (Fig. 3). From our reconstructed liquid we obtain crystallization P-T conditions of 950—1109°C and -1.7 – 7.8 kbar (the small negative pressures being effectively within error of 1 atm; Fig. 11).

Olivine. For mafic enclaves, olivine-liquid equilibria geothermometry of measured olivine and reconstructed liquid compositions yield estimates of crystallization temperatures over the interval of 989—1090 ±19°C (Fig. 11).

Amphibole & Plagioclase: Bimodal and Trimodal Populations. As a whole, amphibole-only thermometry and amphibole-liquid thermobarometry yield crystallization conditions of 719—950°C and 0.2—4.0 kbar (Fig. 11), and liquids ranging from 58-75% SiO_2 (Fig. 3). Similarly, plagioclase-liquid equilibria yield widely ranging compositions and

574 crystallization T-P conditions, 770—1089°C (Fig. 11). These Pl-derived *T* estimates may be
575 maxima for Pl+liq equilibrium, given the findings of Humphreys et al. (2016). But the
576 distributions of crystal compositions (and implied liquids) is not uniform. Chaos Crags
577 amphibole compositions are distinctly bi-modal, while plagioclase compositions are arguably tri-
578 modal, and calculated equilibrium liquids share these distributions (Fig. 12).

579 For amphibole, the felsic mode is somewhat normally distributed and the liquids have
580 73.6 ±0.8 wt.% SiO_2 and 0.4 ±0.2 wt.% MgO, although as hinted at earlier, for these very felsic
581 liquids, our choice of a felsic end-member becomes significant. For example, using a rhyolite
582 from Quinn (2014) we obtain a liquid having 0.9 wt. % MgO at 74 wt. % SiO2, while using a
583 Chaos Crags rhyodacite (and extrapolating to higher-than-observed SiO_2 compositions) we
584 obtain a liquid having 0.3 wt. % MgO at the same SiO_2. Most other oxides are not affected by
585 such a choice, but MgO contents can influence P-T estimates. In this case, the effect is within
586 error of P-T estimation, as the higher MgO case yields a T estimate just 1.3°C higher, while the *P*
587 estimate is fractionally more significant, at 0.6 kbar higher than the low MgO case, but still
588 smaller than the ±1.5 kbar error. The resulting *P-T* conditions for these crystals using the likely
589 more relevant rhyolitic glass compositions from Quinn (2014) are 1.1 ±0.2 kbar, and 790 ±20°C
590 (Fig. 11). The mafic mode of amphibole-saturated liquids is more uniformly distributed with
591 equilibrated liquids having 55-67 wt.% SiO_2 and 2-4 wt.% MgO (mean = 61.8 ±2.5 wt.% SiO_2;
592 3.0 ±0.5 wt.% MgO) and *P-T* conditions of 890-950°C and 1.5-4.5 kbar (mean values of 920
593 ±20°C and 2.6 ±0.7 kbar; Fig. 12). Note that some computed amphibole-equilibrated liquids are
594 more felsic (71-75 wt.% SiO_2) than the rhyodacites that form the bulk of the Chaos Crags domes
595 (Fig. 3), which range to 69.8 wt.% SiO_2, which reflects their equilibration with liquids that exist
596 in the matrices of mineral-melt mixtures.

Plagioclase-equilibrated liquids are even more felsic, as they equilibrate with plagioclase that has a distinct mode at An_{31}, and appear to require liquids quite similar to those produced by Quinn (2014) having 78.7 wt.% SiO_2 (Fig. 3), equilibrating at 780°C, if P = 2 kbar. As noted, there is also a highly mafic mode, centered at An_{92}, that requires liquids with 53 wt.% SiO_2 and 6 wt.% MgO, equilibrating at 1080°C. Finally, there is an intermediate mode at $An_{76\pm3}$, which implies parent liquids having 60 ±1 wt.% SiO_2 and 3.1 ±0.4 wt.% MgO, equilibrating at 1009 ±15°C (Fig. 12). Interestingly, while plagioclase compositions exhibit a continuum, there are a paucity of compositions in the ranges $An_{33\text{-}60}$ and $An_{85\text{-}90}$ (Fig. 12). This implies a paucity of plagioclase-saturated liquids in the respective ranges of 68-78 wt.% SiO_2 and 53-55 wt.%SiO_2.

Agreement of Clinopyroxene and Amphibole Thermobarometry. When averaged, clinopyroxene and amphibole thermobarometers yield remarkably similar P estimates, at 2.1 ± 0.9 kbar and 1.7 ± 1.1 kbar respectively (here we ignore the few clinopyroxene phenocrysts that allowably equilibrate from more mafic liquids, at higher P). As might be expected, amphibole crystallizes at much lower temperatures: mean and median conditions are 812±55°C for amphibole, 1045 ±26°C for clinopyroxene, and 1047 ±39°C for orthopyroxene. But, as noted, amphibole compositions—and their P-T estimates—are distinctly bi-modal: Fig. 11 shows near isobaric crystallization of a subset of amphibole crystals, at 1.2 ±0.2 kbar and 780-880°C, which might represent the P-T conditions of resident felsic magmas prior to interaction with mafic recharge. Finally, we find a compelling convergence in maximum temperatures derived from olivine, plagioclase, and clinopyroxene, reaching 1080-1090°C at nearly every dome (Fig. 13). This seems much too unlikely to be coincidental, and so we infer that 1080-1090°C is the T of recharge magmas as they enter the Chaos Crags shallow storage system.

As noted above, we obtain viable clinopyroxene-equilibrated liquids that mostly have 53-58 wt.% SiO_2 and 3.6-5.0 wt.% MgO, while a few groundmass crystals plausibly form from liquids with 67 wt.% SiO_2 and 2 wt.% MgO. We obtain nearly all these liquids by adding mostly <15% of a rhyodacitic magma to CC-A-I-6. This result is consistent with our finding clinopyroxene only rarely within host felsic lavas, and with clinopyroxene being much less abundant, and sometimes absent, among our most mafic and nearly-aphyric enclaves. But, we might also ask whether any of our clinopyroxene grains might allowably precipitate from the same or similar magmas that apparently precipitate olivine (Fo_{82}) and plagioclase (An_{92}) crystals? We find that most clinopyroxene grains are driven further from equilibrium when either of our >6% mafic magmas (Table 3) are used as an end-member, but the An_{90}-saturated liquid (Table 3) explains a half dozen or so clinopyroxene phenocrysts perfectly well. Using that liquid composition, we must naturally obtain different *P-T* estimates, as dictated by the models, and thermodynamic theory, and we find a mean *P* and *T* of 3.6±0.5 kbar and 1073±7^{o}C, as compared to the 1.9 ± 1.0 kbar and 1037±16^{o}C *P-T* conditions estimated operating on the assumption that all clinopyroxene must form from magmas more felsic than CC-A-I-6. Thus, based on equilibrium tests, we cannot deny that the An_{90}-saturated liquid as a parent for some clinopyroxene grains (although for the majority of measured clinopyroxene compositions, this is not allowable). And, if the An_{90}-saturated liquid is a viable parent for some clinopyroxene grains, then at least some clinopyroxene crystallization may occur closer to 4 kbar, rather than 2 kbar. The An_{90} saturated liquid also can explain the two microphenocrysts that otherwise yield 7-7.5 kbar pressures (Fig. 11), raising their *P*-estimates to ~10 kbar. These differences (~40^{o}C; 1.7-2.5 kbar) represent likely maximum errors related to estimating liquid compositions.

Discussion

The Composition of Recharge Magmas

Our new mineral compositions and tests of equilibrium, as well as petrographic observations and experiments by Quinn (2014), place significant constrain on the compositions of recharge and felsic liquids, and the conditions at which they interacted. For example, we find remarkably similar maximum *T* estimates at most domes, for olivine (1090°C) and plagioclase (1080°C) (Fig. 13), which indicates that each dome eruption was preceded by recharge of very similar magmas that entered the system at very similar temperatures. Maximum T estimates for clinopyroxene range a bit more widely, from 1121-1153°C at Domes A and B, decreasing to 1034°C at Dome F (Fig. 13a), and Dome F also exhibits a lower maximum olivine *T* (1074°C); this T drop may record a subtle change in the deeper recharge staging region. A working hypothesis is that the steady, 1080-1090°C magmas record inputs from a middle-lower crust reservoir at 7-10 kbar (Fig. 11), and that the higher temperatures recorded by some early Cpx may record even deeper levels of recharge (≥7-10 kbar) (Fig. 11). In any case, the most persistent recharge magmas that entered the shallow crust contained 5.5-6.1 wt. % MgO (52-53 wt. % SiO_2) and were intruded at close to 1100°C. This continuity might also be explained by a single recharge magma that drove all six dome eruptions—but in such a case we should perhaps expect a regular cooling trend among maximum T estimates for both of Pl and Ol, which is not observed (Fig. 13).

We also find that the rhyolite liquid compositions obtained by Quinn (2014) work very well as an end-member liquid for describing a range of high-Si Amp and low-An Pl compositions that require liquids more felsic than any observed Chaos Crags whole rock. These ubiquitous plagioclase and amphibole compositions require liquids having 73-78% SiO_2, with

our highest calculated SiO_2 liquid compositions matching well with rhyolite glasses reported by Quinn (2014). But we also find many intermediate-An Pl, intermediate-Si Amp, and low-Fo Ol that would each require liquids of intermediate compositions to exist; we only know that while Chaos Crags lavas are bi-modal, there must have existed, at one point in time, many other liquid compositions which are not reflected in the final eruptive products. To model these intermediate compositions, we assume that recharge magmas interacted with bulk Chaos Crags rhyodacite, rather than a rhyolitic liquid that existed perhaps only as a matrix (Quinn 2014). However, we obtain the same calculated liquids and P-T conditions regardless of the mixing end-member when SiO_2<68 wt. % (due to the relatively linear nature of Chaos Crags compositions). As such, our choice of end-members does not affect our result that mafic and felsic magmas mixed to form new liquid compositions, which then cooled sufficiently to create intermediate composition minerals.

These recharge magmas entered the Chaos Crags system co-saturated with olivine and plagioclase, and at least some were saturated in clinopyroxene, as our most mafic enclaves carry all three of these crystalline phases. These same enclave samples formed from sparsely phyric magmas which appear to have exited a deeper storage zone after rather efficient crystal-liquid separation, and then were quenched as they intruded into a cold and shallow felsic magma reservoir. We surmise that these quenched enclaves were perhaps the first recharge magmas to enter the felsic system.

We should add that magmas with even 6-7% MgO are highly unlikely to represent mantle-derived magmas (Putirka 2017) and so these mafic recharge magmas are themselves differentiated, perhaps at pressures of 7-8 kbar or greater, if the highest *P* estimates from clinopyroxene are indicative (Fig. 11). So why might the repeated batches of recharge have such

688 similar temperatures and composition? The regularity of these magmas would seem to indicate a
689 threshold-driven process, whereby mafic magmas become sufficiently buoyant in the lower crust
690 at 5.5-6.1 wt.% MgO so as to rise into the upper crust, where they re-activate existing, perhaps
691 near-solidus but in any case, un-eruptible rhyodacite magmas.

692 Interestingly, minimum *T* estimates for plagioclase increase through the eruptive
693 sequence (Fig. 13b), and the mean value of rhyodacite-derived Pl temperatures increases from
694 Domes A to F. The simplest explanation is that the first recharge magma interacts with a shallow
695 felsic system at its coolest, while successive recharge magmas invade a progressively hotter
696 felsic reservoir, containing a greater abundance of newly activated and hybridized magmas. We
697 do not have temperatures for Amp from all six domes, but amphibole crystals from domes D-F
698 exhibit a much wider range of crystallization T, extending to much higher temperatures than
699 those estimated for Amp crystals obtained from Dome A host lavas (Fig. 13c). So in Domes D-F,
700 the coolest Amp crystals may record the long-term storage conditions of shallow-level
701 rhyodacite, while Amp crystals that range to higher T record not just recharge and mixing events,
702 but also subsequent crystallization of Amp from hybrid magmas following recharge. These
703 observations imply that mixed magmas (and intermediate liquids) were much more important in
704 the latter half of the eruptive sequence.

705 Pressure estimates of clinopyroxene also show where these recharge magmas came into
706 contact with their felsic hosts. The magmas interacted at $P<4$ kbar, (Fig. 11), which is within
707 experimental and analytical uncertainties of the 1.45 kbar estimated by Quinn (2014). Some low-
708 *T* amphibole compositions that derive from mostly felsic host rhyodacite materials yield mean *P*
709 estimates of ~1 kbar, indicating pre-contact *P* conditions. But we should note that T estimates
710 from rims and cores of amphibole grains are the same within error. For example, at Dome F,

amphibole cores have T=772 ±21°C while rims record a mean *T* of 788 ±8°C. This small increase of T at the rims could indicate rejuvenation of the Dome F felsic materials, but the difference in *T* (15°C) is less than both model error, and 1σ variation of amphibole core estimates. These Amp temperatures overlap with those obtained by low-An Pl, which nominally record temperatures of 730-812°C. These temperatures probably reflect a range of processes from pre-recharge equilibration and crystallization, to rejuvenation, to post-mixing cooling.

Implications

A Model for Magma Mixing and Eruption Triggering Operating at Chaos Crags

Our proposed physical model for the Chaos Crags system is as follows: each of the Chaos Crags eruptions was preceded by the intrusion of mafic recharge magma, of similar composition and temperature. Recharge magmas are supplied from the middle crust, with 5.5-6.1 wt.% MgO, at temperatures near 1100°C, and enter a shallow reservoir centered at depth equivalent to 2 kbar pressure, where they come into contact with cooler, resident felsic magma that has been stored for ca. 190 ka (Klemetti and Clynne 2014). Subsequent cooling and crystallization of these mafic magmas, and magma mixing and further crystallization of mixed magmas, leads in each case to a state of vapor saturation that triggered eruption. The total amount of post-recharge cooling approaches 250°C, similar to that inferred for other Cascade volcanic systems (Putirka 2017). This story is remarkably consistent to Clynne's (1990) model for the 1915 eruption at Lassen Peak, and recent findings at Campi Flegrei, Italy (Stock et al. 2016).

Our model is supportive of Folch and Martí (1998), but varies in that we find evidence for significant post-mixing cooling and crystallization. We surmise that neither mafic recharge nor magma mixing are immediate eruption triggers— if either served as an immediate cause of eruption, one would yield a dearth of intermediate composition magmas, and especially

734 intermediate composition minerals (the opposite of what is observed at Chaos Crags, especially
735 among Pl compositions), and mafic enclaves—the rock record of recharge—should not only be
736 quenched, but preserve only their highest temperatures, not a range of temperatures (unlike the
737 temperature range observed within Chaos Crags enclaves). Some enclaves at Chaos Crags are
738 indeed quenched (aphyric, or preserve only high *T* crystals), but many enclaves contain Cpx, Pl,
739 or Amp crystals that cannot be derived from the felsic host, but still record temperatures that are
740 hundreds of degrees lower than inferred initial recharge temperatures of 1100°C, recorded by Pl,
741 Ol, and Cpx. Figure 13, for example, portrays cooling from 1100°C to < 975^{o}C for mafic
742 enclaves at each dome, and an increasing eruption of mixed liquids that had sufficient time to
743 cool following mixing, so as to precipitate intermediate composition minerals, at a range of
744 temperatures. So, while mafic recharge may have been the ultimate trigger for the 1,103 ±13
745 years BP eruption of the Chaos Crags volcanic sequence, individual eruptions were preceded by
746 significant cooling and crystallization of both recharge and mixed magmas at shallow to
747 moderate depths (Figs. 11, 13). One might then argue, however, that recent recharge-triggered
748 eruptions have already been established elsewhere (e.g., Kent et al. 2010). To this, we have two
749 responses. First, not all eruptions, or eruptive systems need operate identically. Second, the
750 diffusion profile interpretations may be in error. At the Chaos Crags, we have near-homogeneous
751 Ol grains that record 1100^{o}C temperatures coexisting with Amp grains whose Si content is much
752 too low to have equilibrated with host rhyodacite, and that record temperatures as low as 800-
753 900^{o}C; closer analysis of putative recharge-triggered eruptions may reveal substantial delays
754 between recharge and eruption.

755 Our analyses of mineral compositions thus testify to repeated recharge and crystallization
756 of recharge magmas at Chaos Crags. Given that both recharge and mixing are followed by some

757 degree of cooling prior to eruption, we suggest that the immediate cause of each of the dome
758 eruptions was an increase in magmatic overpressure within the chamber, induced by volatile
759 contributions from the shallow crystallization of mafic magma. This would lead to fluid
760 saturation, rapid vesiculation, and an increase in fluid pressure within the host magmas of Chaos
761 Crags, as in the "second boiling" concept of Blake (1984). We cannot discount the possible
762 tectonic triggering mechanisms summarized by Wilson (2017), but the repeated nature of Chaos
763 Crags appears to point instead to an auto-magmatic trigger.
764

765 **Acknowledgements**

766

767 We would like to express our very great appreciation to Michael Clynne for his assistance
768 in the field, as well as the many challenging discussions regarding many of the aspects of this
769 project. This manuscript was greatly improved through reviews from Frank J. Tepley, III, Laura
770 Waters, and Barry I. Cameron. This project was supported by National Science Foundation
771 Award No. 1250323.
772

References

Anderson, J. Lawford, and Smith, Diane R. (1995) The effects of temperature and fO_2 on the Al-in-hornblende barometer. American Mineralogist, 80, 549-559.

Armstrong, J.T. (1995) CITZAF – a package of correction programs for the quantitative electron microbeam X-ray-analysis of thick polished materials, thin-films, and particles. Microbeam Analysis, 4, 177-200.

Bacon, Charles R. (1986) Magmatic inclusions in silicic and intermediate volcanic rocks. Journal of Geophysical Research, 91(B6), 6091-6112.

Bacon, Charles R., and Hirschmann, Marc M. (1988) Mg/Mn partitioning as a test for equilibrium between coexisting Fe-Ti oxides. American Mineralogist, 73, 57-61.

Baker, Don R., and Eggler, David H. (1983) Fractionation paths of Atka (Aleutians) high-alumina basalts: constraints from phase relations. Journal of Volcanology and Geothermal Research, 18, 387-404.

Blake, Stephen. (1984) Volatile oversaturation during the evolution of silicic magma chambers as an eruption trigger. Journal of Geophysical Research, 89(B10), 8237-8244.

Blakely, Richard J., Christiansen, Robert L., Guffanti, Marianne, Wells, Ray E., Donnelly-Nolan, Julie M., Muffler, L.J. Patrick, Clynne, Michael A., and Smith, James G. (1997) Gravity anomalies, Quaternary vents, and Quaternary faults in the southern Cascade Range, Oregon and California: implications for arc and backarc evolution. Journal of Geophysical Research, 102(B10), 22,513-22,527.

Blatter, Dawnika L., and Carmichael, Ian S.E. (2001) Hydrous phase equilibria of a Mexican high-sillica andesite: a candidate for mantle origin? Geochimica et Cosmochimica Acta, 65(21), 4043-4065.

796 Busby, C.J., Hagan, J., Putirka, K., Pluhar, C., Gans, P., Rood, D., DeOeo, S., Skilling, I, and
797 Wagner, D. (2008) The ancestral Cascades arc: Implications for the development of the
798 Sierran microplate and tectonic significance of high K_2O volcanism: in, J. Wright and J.
799 Shervais (eds), Ophiolites, Arcs and Batholiths: Geological Society of America Special
800 Paper 438, 48 p.
801 Carmichael, Ian S.E. (1967) The iron-titanium oxides of salic volcanic rocks and their associated
802 ferromagnesian silicates. Contributions to Mineralogy and Petrology, 14, 36-64.
803 Chou, I-Ming. (1978) Calibration of oxygen buffers at elevated *P* and *T* using the hydrogen
804 fugacity sensor. American Mineralogist, 63, 690-703.
805 Christiansen, R.L., Clynne, M.A., and Muffler, L.J.P. (2002) Geologic Map of the Lassen Peak,
806 Chaos Crags, and Upper Hat Creek area, California. U.S. Geological Survey Geologic
807 Investigations Series I-2723.
808 Clynne, Michael A. (1999) A complex magma mixing origin for rocks erupted in 1915, Lassen
809 Peak, California. Journal of Petrology, 40(1), 105-132.
810 Clynne, M.A., Christiansen, R.L., Trimble, D.A., and McGeehin, J.P. (2008) Radiocarbon dates
811 from volcanic deposits of the Chaos Crags and Cinder Cone eruptive sequences and other
812 deposits, Lassen Volcanic National Park and vicinity, California: U.S. Geological Survey
813 Open-file Report 02-290, 18 p.
814 Clynne, Michael A., and Muffler, L.J. Patrick. (2010) Geologic map of Lassen Volcanic National
815 Park and vicinity, California: U.S. Geological Survey Scientific Investigations Map 2899,
816 scale 1:50 000, 1 sheet, 101 p.

Clynne, Michael A., Robinson, Joel E., Nathenson, Manuel, and Muffler, L.J. Patrick. (2012) Volcano hazards assessment for the Lassen Region, northern California: U.S. Geological Survey Scientific Investigations Report 2012-5176-A, 47 p.

Collins, Sarah J., Davidson, Jon P., Morgan, Daniel J., and Llewellin, Edward W. (2012) Crystals, melt inclusions and magma mingling. Mineralogical Magazine, 76(6), Goldschmidt 2012, Montreal, Canada.

Coombs, Michelle L., Eichelberger, John C., and Rutherford, Malcolm J. (2000) Magma storage and mixing conditions for the 1953-1974 eruptions of Southwest Trident volcano, Katmai National Park, Alaska. Contributions to Mineralogy and Petrology, 140, 99-118.

Cooper, Kari M., and Kent, Adam J.R. (2014) Rapid remobilization of magmatic crystals kept in cold storage. Nature, 506(7489), 480-483.

Costa, Fidel, and Chakraborty, Sumit. (2004) Decadal time gaps between mafic intrusion and silicic eruption obtained from chemical zoning patterns in olivine. Earth and Planetary Science Letters, 227(3-4), 517-530.

Costa, F., Domen, R., Chakraborty, S. (2008) Time scales of magmatic processes from modeling the zoning patterns of crystals. Reviews in Mineralogy and Geochemistry, 69, 545-594.

Daly, R.A. (1911) The Nature of Volcanic Action. Proceedings of the American Academy of Arts and Sciences, 47, 47-122.

DiCarlo, Ida Di, Pichavant, Michel, Rotolo, Silvio G., and Scaillet, Bruno. (2006) Experimental Crystallization of a High-K Arc Basalt: the Golden Pumice, Stromboli Volcano (Italy). Journal of Petrology, 47(7), 1317-1343.

Earthchem. (2002) NAVDAT: The western North American volcanic and intrusive rock database. www.navdat.org.

840 Eichelberger, John C. (1974) Magma contamination within the volcanic pile: origin of andesite
841 and dacite. Geology, 2(1), 29-33.
842 Eichelberger, John C. (1975) Origin of andesite and dacite: Evidence of mixing at Glass
843 Mountain in California and at other circum-Pacific volcanoes. Geological Society of
844 America Bulletin, 86, 1381-1391.
845 Feeley, T.C., Wilson, L.F., and Underwood, S.J. (2008) Distribution and compositions of
846 magmatic inclusions in the Mount Helen dome, Lassen Volcanic Center, California:
847 Insights into magma chamber processes. Lithos, 106, 173-189.
848 Folch, A., and Martí, J. (1998) The generation of overpressure in felsic magma chambers by
849 replenishment. Earth and Planetary Science Letters, 163, 301-314.
850 Fountain, John C. (1979) Geochemistry of Brokeoff Volcano, California. GSA Bulletin, 90(3),
851 294-300.
852 Gaetani, G.A., Grove, T.L., and Bryan, W.B. (1994) 32. Experimental phase relations of basaltic
853 andesite from hole 839B under hydrous and anhydrous conditions. Proceedings of the
854 Ocean Drilling Program, Scientific results, 135, 557-563.
855 Ghiorso, Mark S., and Evans, Bernard W. (2008) Thermodynamics of rhombohedral oxide solid
856 solutions and a revision of the Fe-Ti two-oxide geothermometer and oxygen-barometer.
857 American Journal of Science, 308, 957-1039.
858 Ghiorso, M. S. & Sack, R. O. (1995) Chemical mass-transfer in magmatic processes. 4. A
859 revised and internally consistent thermo-dynamic model for the interpolation and
860 extrapolation of liquid-solid equilibria in magmatic systems at elevated temperatures and
861 pressures. Contributions to Mineralogy and Petrology, 119, 197-212.

862 Green, D.H., Nicholls, I.A., Vilojen, M., and Violjen, R. (1975) Experimental demonstration of
863 the existence of peridotitic liquid in earliest Archean magmatism. Geology 11-14.
864 Grove, T.L., Donnelly-Nolan, J.M., and Housh, T. (1997) Magmatic processes that generate the
865 rhyolite of Glass Mountain, Medicine Lake volcano, N. California. Contributions to
866 Mineralogy and Petrology, 127, 205-223.
867 Grove, T.L., Elkins-Tanton, L.T., Parman, S.W., Chatterjee, N., Müntener, O., and Gaetani, G.A.
868 (2003) Fractional crystallization and mantle-melting controls on calc-alkaline
869 differentiation trends. Contributions to Mineralogy and Petrology, 145, 515-533.
870 Gualda, G.A.R., Ghiroso, M.S., Lemons, R.V., and Carley, T.L. (2012) Rhyolite-MELTS: a
871 modified calibration of MELTS optimized for silica-rich, fluid-bearing magmatic
872 systems. Journal of Petrology, 53, 875-890.
873 Guffanti, M., Clynne, Michael A., Smith, James G., Muffler, L.J.P., and Bullen, Thomas D.
874 (1990) Late Cenozoic volcanism, subduction, and extension in the Lassen Region of
875 California, southern Cascade Range. Journal of Geophysical Research, 95(B12), 19453-
876 19464.
877 Hammer, Julia E., and Rutherford, Malcom J. (2002) An experimental study of the kinetics of
878 decompression-induced crystallization in silicic melt. Journal of Geophysical Research,
879 107(B1), 1-24.
880 Hammer, Julia E., and Rutherford, Malcom J. (2003) Petrologic indicators of preeruption magma
881 dynamics. Geology, 31, 79-82.
882 Hammond, Patrick A., and Taylor, Lawrence A. (1982) The ilmenite / titanomagnetite
883 assemblage: kinetics of re-equilibration. Earth and Planetary Science Letters, 61, 143-
884 150.

885 Heiken, Grant, and Eichelberger, John C. (1980) Eruptions at Chaos Crags, Lassen Volcanic
886 National Park, California. Journal of Volcanology and Geothermal Research, 7, 443-481.
887 Herzberg, C. and O'Hara, M.J. (2002) Plume-associated ultramafic magmas of Phanerozoic age.
888 Journal of Petrology, 43, 1857-1883.
889 Hildreth, Wes. (2007) Quaternary Magmatism in the Cascades – Geologic Perspectives: U.S.
890 Geological Survey Professional Paper 1744, 125 p.
891 Hirschmann, M.M., Ghiorso, M.S., Davis, F.A., Gordon, S.M., Mukherjee, S., Grove, T.L.,
892 Krawczynski, M., Medard, E., and Till, C.B. (2008) Library of Experimental Phase
893 Relations (LEPR): A database and Web portal for experimental magmatic phase
894 equilibria data. Geochemistry, Geophysics, Geosystems, 9(3), 1525-2027,
895 doi:10.1029/2007GC001894.
896 Holtz, Francois, Sato, Hiroaki, Lewis, Jared, Behrens, Harald, and Nakada, Setsuya. (2005)
897 Experimental petrology of the 1991-1995 Unzen dacite, Japan. Part I: phase relations,
898 phase composition and pre-eruptive conditions. Journal of Petrology, 46(2), 319-337.
899 Hootman, Crystal Dawn. (2014) Textural analysis of mafic enclaves as an insight into magma
900 mixing processes at Chaos Crags, Lassen Volcanic Center, California, 165 p. M.S.
901 Thesis. California State University, Sacramento.
902 Housh, Todd B., and Luhr, James F. (1991) Plagioclase-melt equilibria in hydrous systems.
903 American Mineralogist, 76, 477-492.
904 Huppert, Herbert E., Sparks, R. Stephen J., and Turner, J. Stewart. (1982) Effects of volatiles on
905 mixing in calc-alkaline magma systems. Nature, 297, 554-557.

906 Kent, Adam J.R., Darr, Cristina, Koleszar, Alison M., Salisbury, Morgan J., Cooper, Kari M.
907 (2010) Preferential eruption of andesitic magmas through recharge filtering. Nature
908 Geoscience, 3, 631-636.
909 Klemetti, E.W., and Clynne, M.A. (2014) Localized rejuvenation of a crystal mush recorded in
910 zircon temporal and compositional variation at the Lassen Volcanic Center, northern
911 California. PLoS ONE, 9(12), e113157.
912 Leake, Bernard E., Woolley, Alan R., Arps, C.E.S., Birch, W.D., Gilbert, M.C., Grice, J.D.,
913 Hawthorne, F.C., Kato, A., Kisch, H.J., Krivovichev, V.G., Linthout, K., Laird, J.,
914 Mandarino, J., Maresch, W.V., Nickel, E.H., Schumacher, J.C., Stephenson, N.C.N.,
915 Whittaker, E.J.W., and Youzhi, G. (1997) Nomenclature of amphiboles: report of the
916 Subcommittee on Amphiboles of the International Mineralogical Association
917 Commission on New Minerals and Mineral Names. Mineralogical Magazine, 61, 295-
918 321.
919 LeBas, M.J., LeMaitre, R.W., Streckeisen, A., and Zanettin, B. (1986) A chemical classification
920 of volcanic rocks based on the total alkali-silica diagram. Journal of Petrology, 27, 745-
921 750.
922 Lepage, Luc D. (2003) ILMAT: an Excel worksheet for ilmenite-magnetite geothermometry and
923 geobarometry. Computers & Geosciences, 29(5), 673-678.
924 Lesher, C.E., and Spera, F.J. (2015) Thermodynamic and Transport Properties of Silicate Melts
925 and Magma. In: Sigurdsson, H., Houghton, B., Rymer, H., Stix, J., McNutt, S. (eds.), The
926 Encyclopedia of Volcanoes, pp. 113-141.
927 Macdonald, G. (1944) The 1840 eruption and crystal differentiation in the Kilauean magma
928 column (Hawaii). American Journal of Science, 242, 177-189.

929 Macdonald, G.A., and Katsura, T. (1965) Eruption of Lassen Peak, Cascade Range, California,
930 in 1915: example of mixed magmas. Geological Society of America Bulletin, 76, 475-
931 482.
932 Marsh, Bruce D. (1988) Crystal size distribution (CSD) in rocks and the kinetics and dynamics
933 of crystallization. Contributions to Mineralogy and Petrology, 99, 277-291.
934 Martin, Victoria M., Morgan, Daniel J., Jerram, Dougal A., Caddick, Mark J., Prior, David J.,
935 and Davidson, Jon P. (2008) Bang! Month-scale eruption triggering at Santorini Volcano.
936 Science, 321, 1178.
937 Moore, Gordon, and Carmichael, I.S.E. (1998) The hydrous phase equilibria (to 3 kbar) of an
938 andesite and basaltic andesite from western Mexico: constraints on water content and
939 conditions of phenocryst growth. Contributions to Mineralogy and Petrology, 130, 304-
940 319.
941 Muffler, L.J. Patrick, and Clynne, Michael A. (2015) Geologic field-trip guide to Lassen
942 Volcanic National Park and vicinity, California: U.S. Geological Survey Scientific
943 Investigations Report 2015-5067, 67 p.
944 Murata, K.J., and Richter, D.H. (1966) The settling of olivine in the Kilauean magma as shown
945 by lavas of the 1959 eruption. American Journal of Science, 264, 194-203.
946 Neave, D., and Putirka, K. (2017). A new clinopyroxene-liquid barometer, and implications for
947 magma storage pressures under Icelandic rift zones. American Mineralogist, 102, in
948 press.
949 O'Hara, M.J. (1968) Are ocean floor basalts primary magmas? Nature, 220, 683-686.
950 O'Neill, Hugh St. C., and Pownceby, Mark I. (1993) Thermodynamic data from redox reactions
951 at high temperatures. I. An experimental and theoretical assessment of the

952 electrochemical method using stabilized zirconia electrolytes, with revised values for the
953 Fe-"FeO", Co-CoO, Ni-NiO and Cu-Cu_2O oxygen buffers, and new data for the W-WO_2
954 buffer. Contributions to Mineralogy and Petrology, 114(3), 296-314.
955 Pallister, John S., Hoblitt, Richard P., and Reyes, Agnes G. (1992) A basalt trigger for the 1991
956 eruptions of Pinatubo volcano? Nature, 356, 426-428.
957 Peterson, T.D. (1996) A refined technique for measuring crystal size distributions in thin section.
958 Contributions to Mineralogy and Petrology, 90, 36-346.
959 Petrelli, M., Perugini, D., and Poli, G. (2006) Time-scales of hybridization of magmatic enclaves
960 in regular and chaotic flow fields: petrologic and volcanologic implications. Bulletin of
961 Volcanology, 68, 285-293.
962 Petrelli, M., Perugini, D., and Poli, G. (2011) Transition to chaos and implications for time-
963 scales of magma hybridization during mixing processes in magma chambers. Lithos, 125,
964 211-220.
965 Putirka, K. (2016a) Rates and styles of planetary cooling on Earth, Moon, Mars and Vesta, using
966 new models for oxygen fugacity, ferric-ferrous ratios, olivine-liquid Fe-Mg exchange,
967 and mantle potential temperature. American Mineralogist, 101, 819-840.
968 Putirka, K. (2016b) Amphibole thermometers and barometers for igneous systems, and some
969 implications for eruption mechanisms of felsic magmas at arc volcanoes. American
970 Mineralogist, 101, 841-858.
971 Putirka, K., Perfit, M., Ryerson, F.J., and Jackson, M.G. (2007) Ambient and excess mantle
972 temperatures, olivine thermometry, and active vs. passive upwelling. Chemical Geology,
973 241, 177-206.

974 Putirka, K.D. (2008) Thermometers and barometers for volcanic systems, in: K.D. Putirka and F.
975 Tepley (eds), Reviews in Mineralogy and Geochemistry, 69, 61-120.
976 Putirka, Keith. (1999) Clinopyroxene + liquid equilibria to 100 kbar and 2450 K. Contributions
977 to Mineralogy and Petrology, 135, 151-163.
978 Putirka, Keith D. (2005) Igneous thermometers and barometers based on plagioclase + liquid
979 equilibria: Tests of some existing models and new calibrations. American Mineralogist,
980 90, 336-346.
981 Putirka, Keith D. (2017) Down the crater: where magmas are stored and why they erupt.
982 Elements, 13, 11-16.
983 Putirka, Keith D., Canchola, Joe, Rash, Jeffrey, Smith, Oscar, Torrez, Gerardo, Paterson, Scott
984 R., and Ducea, Mihai N. (2014) Pluton assembly and the genesis of granitic magmas:
985 Insights from the GIC pluton in cross section, Sierra Nevada Batholith, California.
986 American Mineralogist, 99(7), 1284-1303.
987 Quinn, Erin T. (2014) Experimental determination of pre-eruptive storage conditions and
988 continuous decompression of rhyodacite magma erupted from Chaos Crags, Lassen
989 Volcanic Center, California, 179 p. M.S. thesis, Humboldt State University.
990 Rader, Erika L., and Larsen, Jessica F. (2013) Experimental phase relations of a low MgO
991 Aleutian basaltic andesite at XH_2O = 0.7-1. Contributions to Mineralogy and Petrology,
992 166, 1593-1611.
993 Richer, Mathieu, Mann, Crystal P., and Stix, John. (2004) Mafic magma injection triggers
994 eruption at Ilopango Caldera, El Salvador, Central America, in: Rose, W.I., Bommer, J.J.,
995 López, D.L., Carr, M.J., and Major, J.J. (eds.), Natural hazards in El Salvador: Boulder,
996 Colorado, Geological Society of America Special Paper 375, 175-189.

997 Ridolfi, F., and Renzulli, A. (2011) Calcic amphiboles in calc-alkaline and alkaline magmas:
998 thermobarometric and chemometric empirical equations valid up to 1,130°C and 2.2 GPa.
999 Contributions to Mineralogy and Petrology, doi: 10.1007/s00410-011-0704-6.
1000 Roeder, P.L., and Emslie, R.F. (1970) Olivine-liquid equilibrium. Contributions to Mineralogy
1001 and Petrology, 29, 275-289.
1002 Rutherford, M.J., Sigurdsson, Haraldur, Carey, Steven, and Davis, Andrew. (1985) The May 18,
1003 1980, eruption of Mt. St. Helen: 1. Melt composition and experimental phase equilibria.
1004 Journal of Geophysical Research, 90(B4), 2929-2947.
1005 Scaillet, Bruno, and Evans, Bernard W. (1999) The 15 June 1991 eruption of Mount Pinatubo. I.
1006 Phase equilibria and pre-eruption P-T-fO_2-fH_2O conditions of the dacite magma. Journal
1007 of Petrology, 40(3), 381-411.
1008 Schmidt, Erica Rose. (2014) Enclave compositions cndicate multiple felsic components at Chaos
1009 Crags, Lassen Volcanic National Park, California, 149 p. M.S. Thesis. California State
1010 University, Sacramento.
1011 Schrecengost, K., Cooper, K.M., Kent, A.J., Huber, C., and Clynne, M.A. (2016) Recycling,
1012 Remobilization, and Eruption of Crystals from the Lassen Volcanic Center. 2016 AGU
1013 Fall Meeting, Abstract No. V51C-01.
1014 Sparks, R.S.J., Sigurdsson, H., and Wilson, L. (1977) Magma mixing – a mechanism for
1015 triggering acid explosive eruptions. Nature, 267, 315-318.
1016 Spera, F.J. (2000) Physical Properties of Magma. In: Encyclopedia of Volcanoes, H. Sigurdsson
1017 (ed.), pp. 171-190.

1018 Stock, M.J., Humphreys, M.C.S., Smith, V.C., Isaia, R., and Pyle, D. (2016) Late-stage volatile
1019 saturation as a potential trigger for explosive volcanic eruptions. Nature Geoscience, 9,
1020 249-255.
1021 Stolper, E. (1980) A phase diagram for mid-ocean ridge basalts: preliminary results and
1022 implications for petrogensis. Contributions to Mineralogy and Petrology, 74, 13-27.
1023 Streck, Martin J., Dungan, Michael A., Malavassi, E., Reagan, Mark K., and Bussy, Francois.
1024 (2002) The role of basalt replenishment in the generation of basaltic andesites of the
1025 ongoing activity at Arenal volcano, Costa Rica: evidence from clinopyroxene and spinel.
1026 Bulletin of Volcanology, 64, 316-327.
1027 Tepley, F.J. III, Davidson, J.P., and Clynne, M.A. (1999) Magmatic interactions as recorded in
1028 plagioclase phenocrysts of Chaos Crags, Lassen Volcanic Center, California. Journal of
1029 Petrology, 40(5), 787-806.
1030 Underwood, S.J., Feeley, T.C., and Clynne, M.A. (2012) Hydrogen isotope investigation of
1031 amphibole and biotite phenocrysts in silicic magmas erupted at Lassen Volcanic Center,
1032 California. Journal of Volcanology and Geothermal Research, 227-228, 32-49.
1033 Venezky, D.Y. and Rutherford, M.J. (1997) Preeruption conditions and timing of dacite-andesite
1034 magma mixing in the 2.2 ka eruption at Mount Rainer. Journal of Geophysical Research,
1035 102(B9), 20069-20086.
1036 Waters, L.E., Andrews, B.J., and Lange, R.A. (2015) Rapid crystallization of plagioclase
1037 phenocrysts in silicic melts during fluid-saturated ascent: phase equilibrium and
1038 decompression experiments. Journal of Petrology, 56(5), 981-1006.
1039 Watson, M.L. (1955) The use of carbon films to support tissue sections for electron microscopy.
1040 Journal of Biophysical and Biochemical Cytology, 1(2), 183-184.

Wallace, G.S., and Bergantz, G.W. (2005) Reconciling heterogeneity in crystal zoning data: An application of shared characteristic diagrams at Chaos Crags, Lassen Volcanic Center, California. Contributions to Mineralogy and Petrology, 149, 98-112.

Wallace, P.J., and Carmichael, I.S.E. (1994) Petrology of Volcán Tequila, Jalisco, Mexico: disequilibrium phenocryst assemblages and evolution of the subvolcanic magma system. Contributions to Mineralogy and Petrology, 117, 345-361.

Wilson C.J.N. (2017) Volcanoes: characteristics, tipping points and those pesky unknown unknowns. Elements, 13, 41-46.

Woods, Andrew W., and Cowan, Alexander. (2009) Magma mixing triggered during volcanic eruptions. Earth and Planetary Science Letters, 288, 132-137.

1052 **List of Figure Captions**

1053

1054 Figure 1. Simplified geologic map of the Chaos Crags [after Christiansen et al. (2002)] overlain
1055 on 1 MOA Shasta Co. DEM (USGS National Elevation Dataset).

1056

1057 Figure 2. Wt.% SiO_2 vs. measured mol% An (plagioclase) within natural Chaos Crags samples
1058 from this study and experimental plagioclase from referenced studies. Experimental plagioclase
1059 are equilibrated over the range of 750-1125°C, 0.01-2.5 kbar, and 1.2-5.3 wt.% H_2O; red
1060 rectangle illustrates an equilibrium range of An as extrapolated from experimental studies.
1061 Measured plagioclase not in equilibrium with the bulk rock composition in which they are
1062 contained are present within both mafic enclaves and host lavas (note the bimodal distribution of
1063 bulk rock compositions as compared to wide range of An contents), as illustrated by blue arrows.

1064

1065 Figure 3. A comparison of SiO_2 vs. (A) MgO and (B) K_2O for natural whole rock compositions
1066 at Chaos Crags (light open gray circles) and liquids that are calculated to be in equilibrium with
1067 olivine (Ol) of compositions ranging from Fo_{69}-Fo_{82}, clinopyroxene (Cpx; nominally crystallizes
1068 at 0-4 kbar), Amphibole (Amp; crystallizing at 0-4 kbar), and liquids saturated with plagioclase
1069 (Pl) of compositions An_{92} and An_{33} (not all calculated Pl-saturated liquids are shown, as they
1070 yield a continuum between these two end members; see Fig. 12). All calculated liquids use a
1071 Chaos Crags rhyodacite whole rock as a felsic end-member, until the require liquid compositions
1072 are more felsic than observed whole rock compositions, in which case we use a rhyolite liquid
1073 with 78% SiO_2 from Quinn (2014) as a mixing end-member. The circled gray triangles show the
1074 shift in MgO contents if we were to use a linear extrapolation along the observed whole rock

trend. For all other elements, the offset is trivial, and the error due to the choice of felsic end-members is less than the size of the plotted symbols when SiO_2<68% (see text for details). Also shown is the nearly aphyric mafic enclave CC-A-I-6, which is a useful end-member composition for calculating equilibrium liquids (Table 3), two of the Quinn (2014) rhyolite liquid compositions, and the calculated liquids as modeled using our lowest observed An contents (An33) for plagioclase crystals that occur in the host rhyodacite whole rocks.

Figure 4. Variations in wt.% SiO_2 and wt.% MgO by dome (A-F). Note that over the course of the eruption sequence, host lavas decrease in wt.% SiO_2 and increase in wt.% MgO; the opposite trends are evident in mafic enclaves.

Figure 5. Compositional variations in measured pyroxenes. Pyroxene compositions measured from host lavas are represented in light grey; pyroxene compositions measured from mafic enclaves are represented in dark grey.

Figure 6. BSE images of disequilibrium mineral assemblage present within selected Chaos Crags mafic enclaves. Replacement of hornblende by clinopyroxene and sieve-textured zoned plagioclase phenocryst present within Dome D mafic enclave (a). Coexisting quartz and olivine phenocryst within Dome A mafic enclave, note pyroxene reaction rim surrounding quartz (b). Highly reacted sieve-textured plagioclase within Dome B mafic enclave (c). Cpx = clinopyroxene, gl = glass, Pl = plagioclase, hbl = hornblende, mt = magnetite, qtz = quartz, opx = orthopyroxene.

Figure 7. Frequency distributions of olivine Fo contents within Chaos Crags mafic enclaves. Fo content = 100 · [Mg/(Mg + Fe)].

Figure 8. Classification of amphiboles present within Chaos Crags eruptive products. Amphibole compositions measured from host lavas are represented in light grey; amphibole compositions measured from mafic enclaves are represented in dark grey [after Leake et al. (1997)].

Figure 9. Frequency distributions of Pioclase An contents within Chaos Crags eruptive products. Plagioclase compositions measured from host lavas are represented in white with black outlines; plagioclase compositions measured from mafic enclaves are represented in grey. An component = Ca/(Ca + Na).

Figure 10. Isobaric (P=2 kbar) crystallization temperature (°C) and fO_2 estimates of Chaos Crags eruptive products calculated using Fe-Ti oxide geothermobarometer of Ghiorso and Evans (2008); σ_{est} for Fe-Ti oxides = ±51°C. Co-CoO and Ni-NiO oxygen buffers calculated using O'Neill and Pownceby (1993). MH, MnO-Mn_3O_4, and QFM oxygen buffers calculated using Chou (1978).

Figure 11. Temperature vs. pressure estimates derived from clinopyroxene-liquid equilibria, amphibole-liquid equilibria, and amphibole compositions only. Also shown are ranges of T estimates deriving from olivine (green), enclave-hosted plagioclase (dark gray) and rhyodacite hosted plagioclase light gray, with lines indicating the complete Ol and Pl temperature ranges. Error on individual *P-T* estimates is shown. Cpx and Amp pressures are effectively equivalent in

range (excepting the two high-P Cpx estimates), indicating that most crystallization of all phases occurs at P< 4 kbar, and perhaps, if mean values are most accurate, at mostly 2 kbar pressures. The deeper P estimates of 7-7.5 kbar (which increase to 10 kbar if we use the An_{92}-saturated liquid from Table 3, which is allowably in equilibrium with these crystals) may represent the depths (25-35 km) at which mafic recharge magmas are fractionated (from some higher MgO parent, which almost assuredly exists; Putirka 2017) as well as the depths from which recharge magmas are delivered from, prior to being emplaced at shallow depths. This would place the mafic storage region (pre-recharge) in the lower crust or upper mantle.

Figure 12. Histograms (n = 305) of (A) Anorthite (An) content of plagioclase, (B) SiO_2 contents of liquids equilibrated with such plagioclase, that are also consistent with Chaos Crags whole rock compositions (see Fig. 3), and (C) temperature estimates for plagioclase + liquid equilibrium. Black lines connect corresponding An–SiO_2^{liq}–*T* values for what appear to be three distinct modes of Pl compositions.

Figure 13. Temperature estimates by Dome for (A) Olivine (n = 275) and Clinopyroxene (n = 103), (B) Plagioclase, with enclave- and felsic host-derived Pl crystals distinguished (n=305), and (C) Amphibole (n = 60). Upper dashed line at 1090°C indicates a typical maximum *T* estimate for both Ol and Pl at most domes. Lower dashed line at 820°C indicates maximum *T* estimate for amphibole grains hosted by rhyodacite; mafic enclave-derived Amp range to much higher temperatures, but also trend to similarly low values of ca. 740°C, the latter of which are likely derived by mixing with rhyodacite host magmas. In (B), minimum Pl *T* estimates increase monotonically as the eruptive sequence progresses from Domes B to F, which probably represent

1144 the heating of resident, shallowly-stored felsic magma by the repeated input of high *T* recharge
1145 magmas.

This is a preprint, the final version is subject to change, of the American Mineralogist (MSA)
Cite as Authors (Year) Title. American Mineralogist, in press.
DOI: https://doi.org/10.2138/am-2018-6058

1146 **List of Tables**

1147

1151

This is a preprint, the final version is subject to change, of the American Mineralogist (MSA)
Cite as Authors (Year) Title. American Mineralogist, in press.
DOI: https://doi.org/10.2138/am-2018-6058

1152 **List of Appendices**

1153

1154 Appendix A. Whole Rock Measured Major Oxide Compositions

1155 Appendix B. Fe-Ti Oxides Measured Compositions

1156 Appendix C. Orthopyroxene Measured Compositions

1157 Appendix D. Clinopyroxene Measured Compositions

1158 Appendix E. Olivine Measured Compositions

1159 Appendix F. Amphibole Measured Compositions

1160 Appendix G. Plagioclase Measured Compositions

This is a preprint, the final version is subject to change, of the American Mineralogist (MSA)
Cite as Authors (Year) Title. American Mineralogist, in press.
DOI: https://doi.org/10.2138/am-2018-6058

1161 Table 1. Methods and Conditions for Quantitative Chemical Analyses of Mineral Phases

Mineral Phase Evaluated	Cpx	Amp	Il	Mt	Ol	Opx	Pl
Major Oxide Compositions Analyzed[1]	SiO_2, TiO_2, Al_2O_3, FeO_{tot}, MnO, MgO, CaO, Na_2O, K_2O, and Cr_2O_3	SiO_2, TiO_2, Al_2O_3, FeO_{tot}, MnO, MgO, CaO, Na_2O, K_2O, and Cr_2O_3	SiO_2, TiO_2, Al_2O_3, FeO_{tot}, MnO, MgO, CaO, Na_2O, K_2O, and Cr_2O_3	SiO_2, TiO_2, Al_2O_3, FeO_{tot}, MnO, MgO, V_2O_3, and Cr_2O_3	SiO_2, TiO_2, Al_2O_3, FeO_{tot}, MnO, MgO, CaO, Na_2O, K_2O, and Cr_2O_3	SiO_2, TiO_2, Al_2O_3, FeO_{tot}, MnO, MgO, CaO, Na_2O, K_2O, and Cr_2O_3	SiO_2, TiO_2, Al_2O_3, FeO_{tot}, MgO, CaO, Na_2O, and K_2O
Na and K Analyzed First?	Yes	Yes	n/a	n/a	Yes	Yes	Yes
Beam Diameter	1 μm	1 μm	<1 μm	<1 μm	1 μm	1 μm	10 μm
Beam Current	10 nA (UCD) 15 nA (USGS)	15 nA	25 nA	25nA	10 nA (UCD) 15 nA (USGS)	10 nA (UCD) 15 nA (USGS)	10 nA (UCD) 15 nA (USGS)
Dwell Tim	10 s	10 s	10-20 s	10-20 s	10 s	10 s	20-40 s
Accelerating Voltage	15 kV	15 kV	15 kV	15 kV	15 kV	15 kV	15 kV

[1]Relative Error Estimates (in wt.%) are: 0.32% SiO_2, 0.03% TiO_2, 0.16% Al_2O_3, 0.16% FeO_{tot}, 0.16% MgO, 0.04% MnO, 0.21% CaO, 0.08% Na_2O, 0.04% K_2O, 0.06% P_2O_5, 0.05% NiO, 0.06% V_2O_3 and 0.02% Cr_2O_3.

1162
1163

1164

Table 3. End-member and Parent Magma Compositions

	SiO_2	TiO_2	Al_2O_3	FeOt	MnO	MgO	CaO	Na_2O	K_2O
Lassen Mafic End-member[1]	52.4	0.7	15.2	8.1	0.1	10.1	10.3	2.4	0.6
Chaos Crags Mafic end-member[2]	53.4	0.7	19.2	8.3	0.1	5.0	9.6	2.9	0.7
Rhyodacite end-member[3]	68.0	0.4	15.7	3.5	0.1	1.6	3.7	4.1	2.6
High-K andesite end-member[4]	61.4	0.9	17.8	5.2	0.1	1.9	4.5	4.9	2.7
Low Mg# Andesite end-member[5]	54.6	0.8	19.5	8.0	0.1	3.8	8.9	3.1	0.8
Parent Magma high Fo82 Ol[6]	53.1	0.7	18.0	8.2	0.1	6.6	9.8	2.8	0.6
Parent Magma of An92 Pl[7]	52.8	0.4	19.3	8.0	0.1	6.1	10.3	2.4	0.6
Resident Felsic magma (An30 Parent)[8]	78.3	0.2	13.2	0.01	0.01	0.04	0.02	4.8	3.4

1. Sample LC84-650A (Earthchem), whole rock composition from 27 Ka Lassen Peak, used as a mafic end-member.
2. Sample CC-A-I-6, a nearly aphyric (<1% crystals) mafic enclave from Dome A, that explains most Cpx and Ol compositions.
3. Rhyodacite from Chaos Crags (CC-D-I-2) used as a felsic end-member, added to CC-A-I-6 to explain most mineral compositions.
4. High K_2O end-member andesite (sample LC84-634) used to explain some low Fo (Fo_{70}) Ol grains.
5. Low Mg# andesite used to explain some low Fo (Fo_{70}) compositions.
6. Parent magma for Ol crystals with maximum Fo contents (Fo_{82}), obtained by mixing CC-A-I-6 with LC84-650A.
7. Parent magma for maximum An content Pl (An_{92-93}); derived from Sisson and Grove (1993) experiments that precipitate similarly high-An content Pl; this composition can also explain Fo_{82} Ol.
8. Parent magma to low-An Pl (An_{30}), not observed as a whole rock at Chaos Crags.

1165

This is a preprint, the final version is subject to change, of the American Mineralogist (MSA)
Cite as Authors (Year) Title. American Mineralogist, in press.
DOI: https://doi.org/10.2138/am-2018-6058

Table 1. Methods and Conditions for Quantitative Chemical Analyses of Mineral Phases

Mineral Phase Evaluated	Cpx	Amp	Il	Mt	Ol	Opx	Pl
Major Oxide Compositions Analyzed[1]	SiO_2, TiO_2, Al_2O_3, FeO_{tot}, MnO, MgO, CaO, Na_2O, K_2O, and Cr_2O_3	SiO_2, TiO_2, Al_2O_3, FeO_{tot}, MnO, MgO, CaO, Na_2O, K_2O, and Cr_2O_3	SiO_2, TiO_2, Al_2O_3, FeO_{tot}, MnO, MgO, CaO, Na_2O, K_2O, and Cr_2O_3	SiO_2, TiO_2, Al_2O_3, FeO_{tot}, MnO, MgO, V_2O_3, and Cr_2O_3	SiO_2, TiO_2, Al_2O_3, FeO_{tot}, MnO, MgO, CaO, Na_2O, K_2O, and Cr_2O_3	SiO_2, TiO_2, Al_2O_3, FeO_{tot}, MnO, MgO, CaO, Na_2O, K_2O, and Cr_2O_3	SiO_2, TiO_2, Al_2O_3, FeO_{tot}, MgO, CaO, Na_2O, and K_2O
Na and K Analyzed First?	Yes	Yes	n/a	n/a	Yes	Yes	Yes
Beam Diameter	1 μm	1 μm	<1 μm	<1 μm	1 μm	1 μm	10 μm
Beam Current	10 nA (UCD) 15 nA (USGS)	15 nA	25 nA	25nA	10 nA (UCD) 15 nA (USGS)	10 nA (UCD) 15 nA (USGS)	10 nA (UCD) 15 nA (USGS)
Dwell Tim	10 s	10 s	10-20 s	10-20 s	10 s	10 s	20-40 s
Accelerating Voltage	15 kV	15 kV	15 kV	15 kV	15 kV	15 kV	15 kV

[1]Relative Error Estimates (in wt.%) are: 0.32% SiO_2, 0.03% TiO_2, 0.16% Al_2O_3, 0.16% FeO_{tot}, 0.16% MgO, 0.04% MnO, 0.21% CaO, 0.08% Na_2O, 0.04% K_2O, 0.06% P_2O_5, 0.05% NiO, 0.06% V_2O_3 and 0.02% Cr_2O_3.

This is a preprint, the final version is subject to change, of the American Mineralogist (MSA)
Cite as Authors (Year) Title. American Mineralogist, in press.
DOI: https://doi.org/10.2138/am-2018-6058

Table 2. Estimated Mineral Modal Abundances of Chaos Crags Eruptive Products

Sample No.	Sample Type	Estimated Modal % Phenocrysts	Estimated Modal % Disequilibrium Phenocrysts	Estimated Modal % Quartz (of total phenocrysts)
CC-A-H-1	Host Lava	21	1	9.52
CC-A-I-3 rim	Mafic Enclave	17	3	--
CC-A-I-3 core	Mafic Enclave	17	2	--
CC-A-I-6 rim	Mafic Enclave	1	< 1	--
CC-A-I-6 core	Mafic Enclave	< 1	< 1	--
CC-A-I-9 rim	Mafic Enclave	10	7	1.41
CC-A-I-9 core	Mafic Enclave	12	9	2.86
CC-A-I-12 rim	Mafic Enclave	4	2	--
CC-A-I-12 core	Mafic Enclave	3	1	--
CC-UPF-I-1 rim	Mafic Enclave	6	5	--
CC-UPF-I-1 core	Mafic Enclave	6	5	--
CC-B-H-1	Host Lava	37	5	6.86
CC-B-I-9 outer rim	Mafic Enclave	10	9	1.01
CC-B-I-9 middle rim	Mafic Enclave	1	1	--
CC-B-I-9 inner rim	Mafic Enclave	< 1	< 1	--
CC-B-I-9 outer core	Mafic Enclave	1	1	--
CC-B-I-9 inner core	Mafic Enclave	< 1	< 1	--
CC-B-I-10 rim	Mafic Enclave	< 1	< 1	--
CC-B-I-10 core	Mafic Enclave	2	2	1.08
CC-C-H-1	Host Lava	79	8	17.50
CC-C-I-1 rim	Mafic Enclave	3	2	--
CC-C-I-1 core	Mafic Enclave	5	3	< 1
CC-C-I-11 rim	Mafic Enclave	5	3	2.38
CC-C-I-11 core	Mafic Enclave	7	4	1.16
CC-C-I-11 intra-enclave	Mafic Enclave	3	1	--
CC-D-H-1	Host Lava	35	8	11.76
CC-D-I-1 rim	Mafic Enclave	10	8	2.19
CC-D-I-1 core	Mafic Enclave	5	3	1.54
CC-D-I-2 core	Mafic Enclave	15	12	2.86
CC-D-I-4 rim	Mafic Enclave	3	1	--
CC-D-I-4 core	Mafic Enclave	5	1	--
CC-D-I-5 rim	Mafic Enclave	1	< 1	--
CC-D-I-5 core	Mafic Enclave	3	1	--
CC-D-I-6 rim	Mafic Enclave	2	2	--
CC-D-I-6 core	Mafic Enclave	1	< 1	--
CC-E-H-1	Host Lava	40	10	7.95
CC-E-I-10 rim	Mafic Enclave	2	2	< 1
CC-E-I-10 core	Mafic Enclave	6	5	--
CC-E-I-11 rim	Mafic Enclave	10	8	4.11
CC-E-I-11 core	Mafic Enclave	5	3	1.40
CC-E-I-12 outer rim	Mafic Enclave	7	6	--

CC-E-I-12 inner rim	Mafic Enclave	10	7	--
CC-E-I-12 core	Mafic Enclave	5	3	--
CC-E-I-13 rim	Mafic Enclave	10	9	< 1
CC-E-I-13 core	Mafic Enclave	5	4	< 1
CC-E-I-14 rim	Mafic Enclave	15	7	--
CC-E-I-14 core	Mafic Enclave	10	2	--
CC-E-I-15 rim	Mafic Enclave	12	10	--
CC-E-I-15 core	Mafic Enclave	15	12	< 1
CC-E-I-16 rim	Mafic Enclave	5	4	4.08
CC-E-I-16 core	Mafic Enclave	5	4	1.67
CC-E-I-18 rim	Mafic Enclave	17	12	1.49
CC-E-I-18 core	Mafic Enclave	12	9	--
CH-CC-08-15 rim	Mafic Enclave	1	1	--
CC-F-H-2	Host Lava	40	10	9.09
CC-F-I-3 rim	Mafic Enclave	7	3	--
CC-F-I-3 core	Mafic Enclave	1	1	--
CC-F-I-10 rim	Mafic Enclave	10	9	2.25
CC-F-I-10 core	Mafic Enclave	10	7	--
CC-F-I-11 rim	Mafic Enclave	20	18	1.14
CC-F-I-11 core	Mafic Enclave	15	14	1.28
CC-F-I-13 rim	Mafic Enclave	5	4	4.88
CC-F-I-13 core	Mafic Enclave	10	9	2.41
CC-F-I-14 rim	Mafic Enclave	3	3	1.23
CH-CC-09-05 rim	Mafic Enclave	3	3	--
CH-CC-09-05 core	Mafic Enclave	1	1	--

This is a preprint, the final version is subject to change, of the American Mineralogist (MSA)
Cite as Authors (Year) Title. American Mineralogist, in press.
DOI: https://doi.org/10.2138/am-2018-6058

Estimated Modal % Plagioclase (of total phenocrysts)	Estimated Modal % Pyroxene (of total phenocrysts)	Estimated Modal % Olivine (of total phenocrysts)	Estimated Modal % Hornblende (of total phenocrysts)	Estimated Modal % Biotite (of total phenocrysts)
71.43	--	--	9.52	9.52
68.52	--	--	31.48	--
68.52	--	--	31.48	--
49.08	1.84	--	49.08	--
51.28	1.28	--	47.44	--
77.46	2.82	1.41	16.90	--
71.43	4.29	7.14	14.29	--
78.57	17.14	4.29	--	--
71.43	21.43	7.14	--	--
83.33	15.00	1.67	--	--
78.13	18.75	3.13	--	--
60.36	13.72	--	16.46	2.61
45.45	--	3.03	50.51	--
51.02	2.04	1.02	45.92	--
56.82	2.27	1.14	39.77	--
47.37	3.16	2.11	47.37	--
51.02	2.04	1.02	45.92	--
46.63	< 1	1.04	51.81	--
54.05	< 1	1.08	43.24	--
67.50	< 1	--	11.33	3.50
68.42	10.53	--	21.05	--
61.86	12.37	2.06	23.71	--
71.43	5.95	2.38	17.86	--
63.95	8.14	3.49	23.26	--
55.56	11.11	5.56	27.78	--
75.29	< 1	--	10.00	2.35
80.29	10.22	2.92	4.38	--
69.23	18.46	7.69	3.08	--
78.57	14.29	--	2.86	1.43
69.45	< 1	--	29.85	< 1
64.87	2.51	--	30.11	2.51
54.55	--	--	45.45	< 1
55.45	--	--	43.56	< 1
--	70.65	--	27.17	2.17
--	66.45	--	33.22	< 1
73.86	1.14	--	13.64	3.41
73.53	10.29	--	14.71	1.00
76.27	8.47	--	11.86	3.39
61.64	2.74	--	30.14	1.37
62.94	2.80	2.10	30.77	--
77.76	15.55	< 1	6.22	< 1

78.13	18.75	1.56	1.56	--
83.33	10.61	3.03	3.03	--
86.61	4.72	--	7.87	< 1
83.33	4.17	--	12.50	--
79.37	11.11	1.59	7.94	--
72.58	19.35	4.84	3.23	--
62.50	3.57	1.79	26.79	5.36
62.11	3.11	1.55	26.40	6.21
81.63	6.12	4.08	4.08	--
66.67	11.67	5.00	10.00	5.00
74.63	10.45	--	8.96	4.48
75.81	16.13	--	4.84	3.23
91.67	1.67	--	6.67	--
73.86	1.14	--	14.77	1.14
71.43	--	--	28.57	--
71.43	--	--	28.57	--
67.57	1.13	< 1	28.15	< 1
65.22	2.17	1.09	30.43	1.09
56.82	2.27	--	39.77	--
57.69	2.56	--	38.46	--
73.17	--	--	20.73	1.22
72.29	--	--	24.10	1.20
74.07	6.17	--	18.52	--
57.29	1.04	--	41.67	--
63.83	2.13	1.06	31.91	1.06

This is a preprint, the final version is subject to change, of the American Mineralogist (MSA)
Cite as Authors (Year) Title. American Mineralogist, in press.
DOI: https://doi.org/10.2138/am-2018-6058

Table 3. End-member and Parent Magma Compositions

	SiO_2	TiO_2	Al_2O_3	FeOt	MnO	MgO	CaO	Na_2O	K_2O
Lassen Mafic End-member[1]	52.4	0.7	15.2	8.1	0.1	10.1	10.3	2.4	0.6
Chaos Crags Mafic end-member[2]	53.4	0.7	19.2	8.3	0.1	5.0	9.6	2.9	0.7
Dacite end-member[3]	68.0	0.4	15.7	3.5	0.1	1.6	3.7	4.1	2.6
High-K andesite end-member[4]	61.4	0.9	17.8	5.2	0.1	1.9	4.5	4.9	2.7
Low Mg# Andesite end-member[5]	54.6	0.8	19.5	8.0	0.1	3.8	8.9	3.1	0.8
Parent Magma high Fo82 Ol[6]	53.1	0.7	18.0	8.2	0.1	6.6	9.8	2.8	0.6
Parent Magma of An92 Pl[7]	52.8	0.4	19.3	8.0	0.1	6.1	10.3	2.4	0.6
Resident Felsic magma (An30 Parent)[8]	78.3	0.2	13.2	0.01	0.01	0.04	0.02	4.8	3.4

1. Sample LC84-650A (Earthchem), whole rock composition from 27 Ka Lassen Peak, used as a mafic end-member.
2. Sample CC-A-I-6, a nearly aphyric (<1% crystals) mafic enclave from Dome A, that explains most Cpx and Ol compositions.
3. Dacite from Chaos Crags (CC-D-H-2) used as a felsic end-member, added to CC-A-I-6 to explain most mineral compositions.
4. High K_2O end-member andesite (sample LC84-634) used to explain some low Fo (Fo_{70}) Ol grains.
5. Low Mg# andesite used to explain some low Fo (Fo_{70}) compositions.
6. Parent magma for Ol crystals with maximum Fo contents (Fo_{82}), obtained by mixing CC-A-I-6 with LC84-650A.
7. Parent magma for maximum An content Pl ($An_{92\text{-}93}$); derived from Sisson and Grove (1993) experiments that precipitate similarly high-An content Pl; this composition can also explain Fo_{82} Ol.
8. Parent magma to low-An Pl (An_{30}), not observed as a whole rock at Chaos Crags.

This is a preprint, the final version is subject to change, of the American Mineralogist (MSA)
Cite as Authors (Year) Title. American Mineralogist, in press.
DOI: https://doi.org/10.2138/am-2018-6058

Figure 1

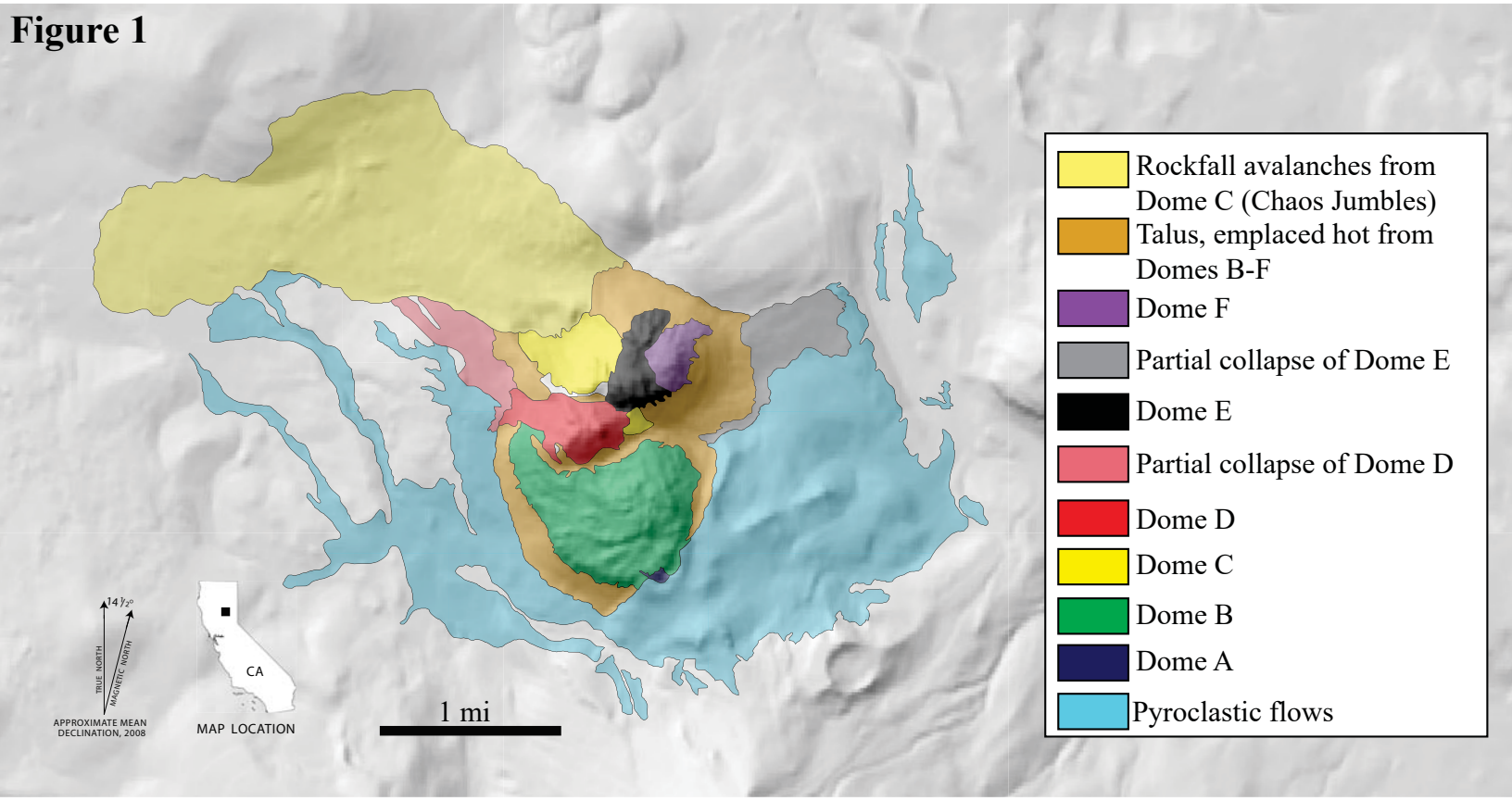

This is a preprint, the final version is subject to change, of the American Mineralogist (MSA)
Cite as Authors (Year) Title. American Mineralogist, in press.
DOI: https://doi.org/10.2138/am-2018-6058

Figure 2

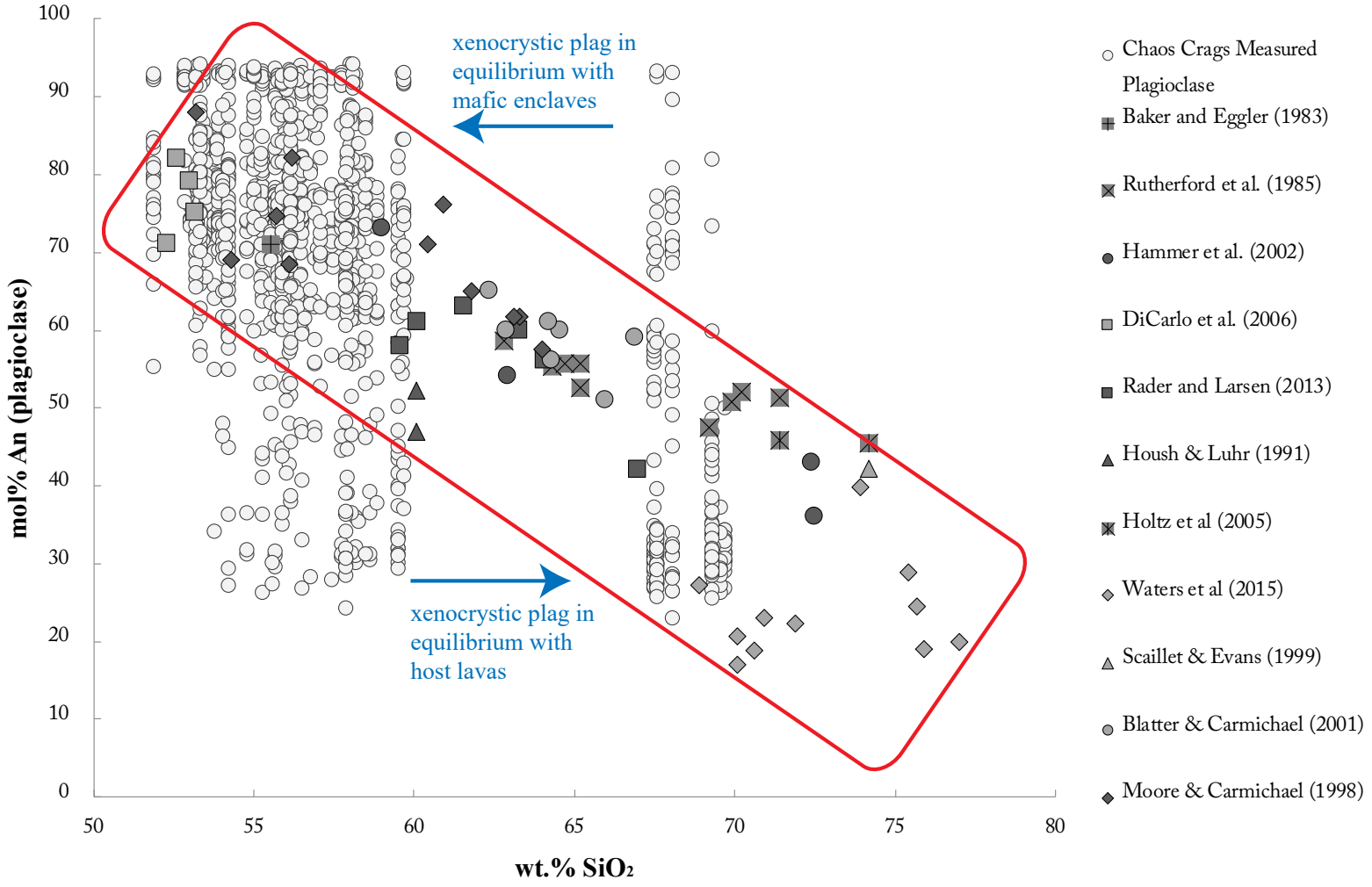

This is a preprint, the final version is subject to change, of the American Mineralogist (MSA)
Cite as Authors (Year) Title. American Mineralogist, in press.
DOI: https://doi.org/10.2138/am-2018-6058

Figure 3

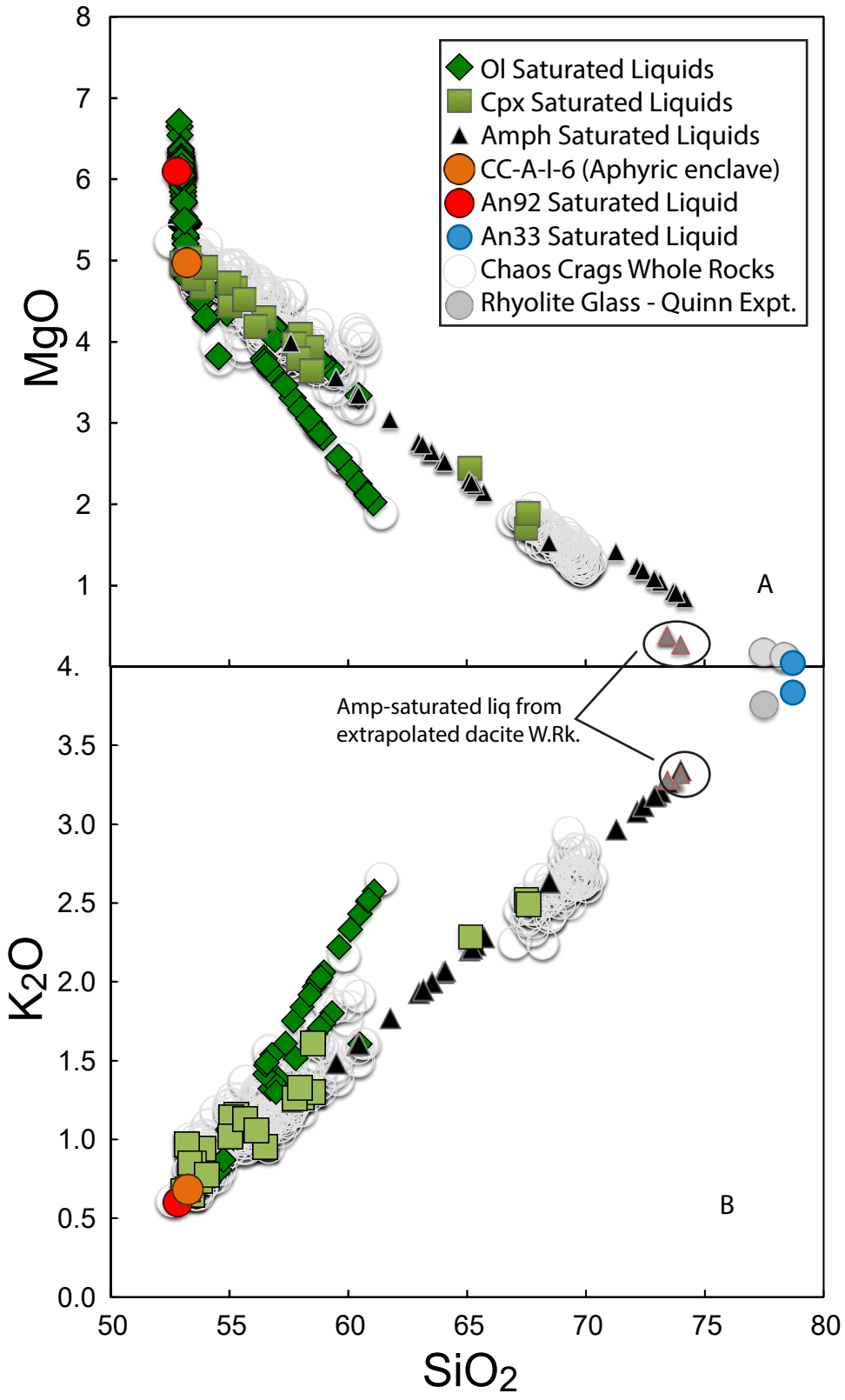

This is a preprint, the final version is subject to change, of the American Mineralogist (MSA)
Cite as Authors (Year) Title. American Mineralogist, in press.
DOI: https://doi.org/10.2138/am-2018-6058

Figure 4

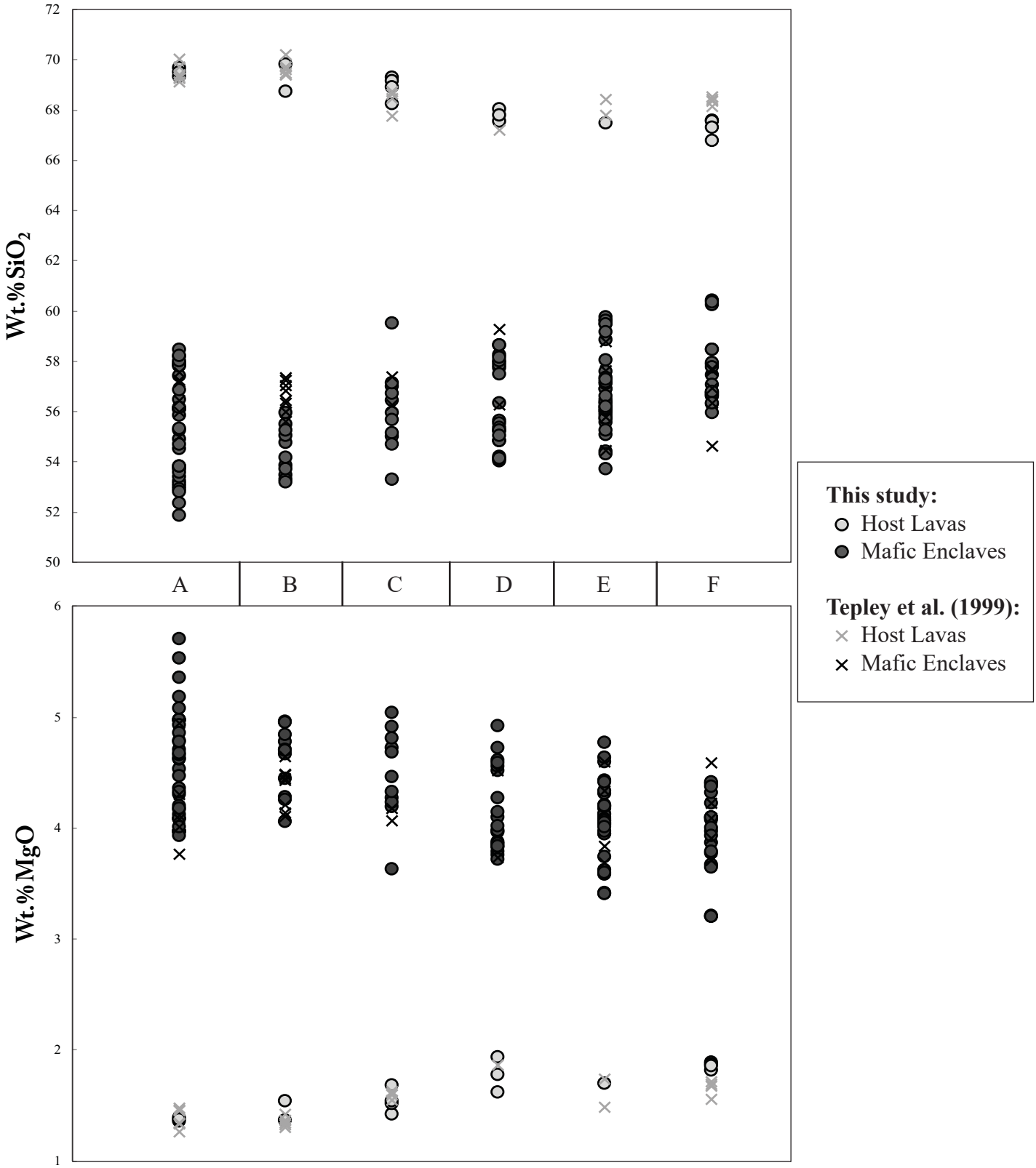

This is a preprint, the final version is subject to change, of the American Mineralogist (MSA)
Cite as Authors (Year) Title. American Mineralogist, in press.
DOI: https://doi.org/10.2138/am-2018-6058

Figure 5

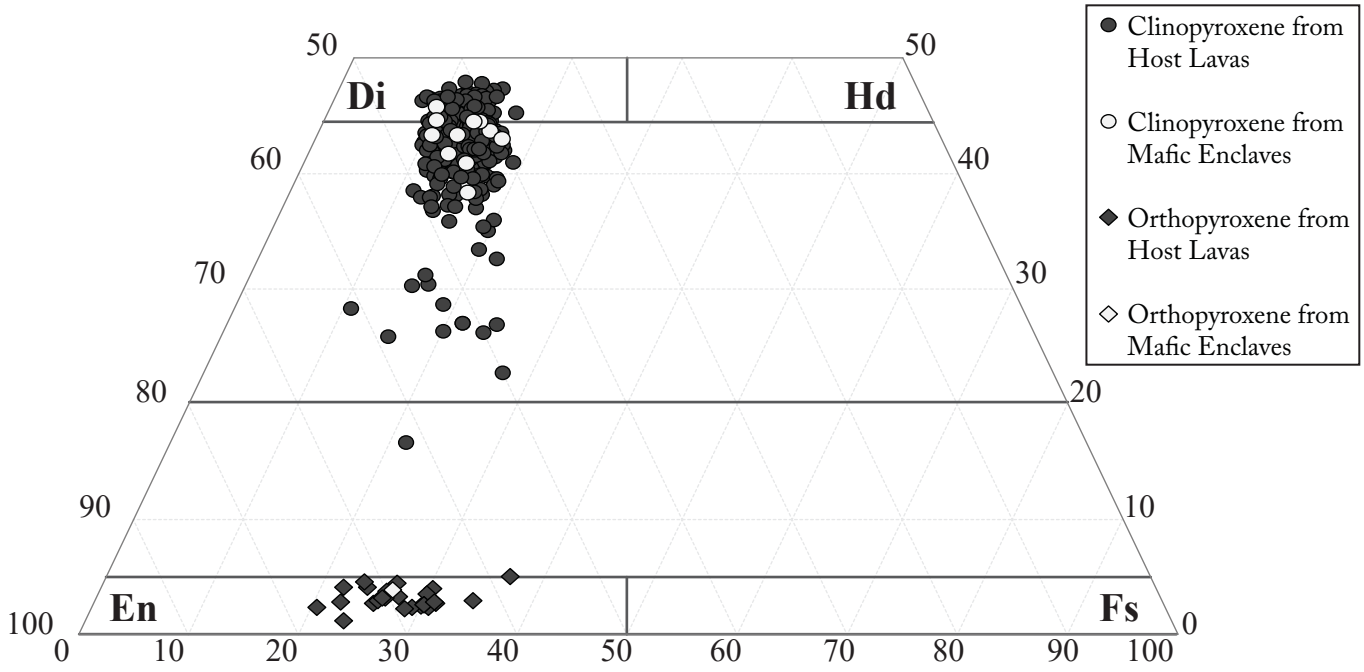

This is a preprint, the final version is subject to change, of the American Mineralogist (MSA)
Cite as Authors (Year) Title. American Mineralogist, in press.
DOI: https://doi.org/10.2138/am-2018-6058

Figure 6

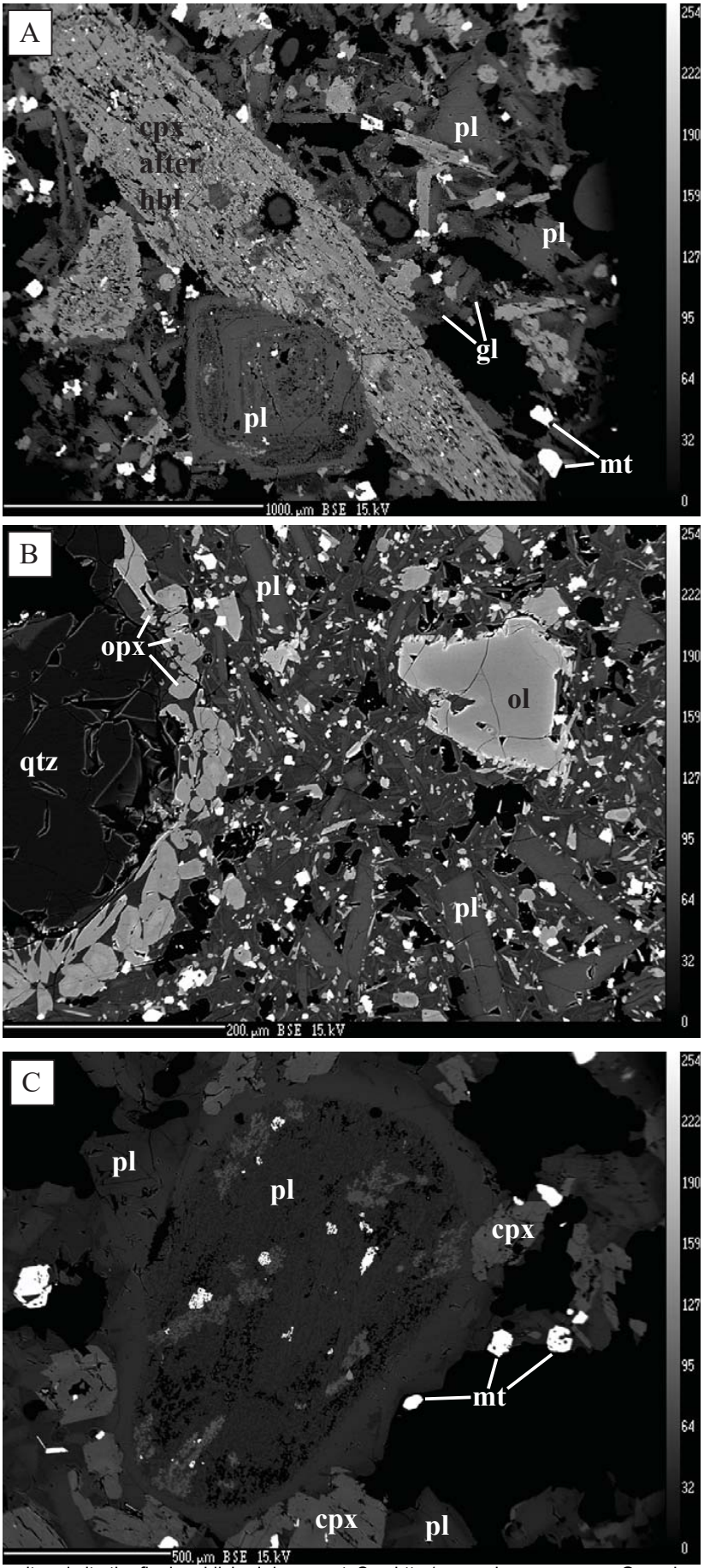

This is a preprint, the final version is subject to change, of the American Mineralogist (MSA)
Cite as Authors (Year) Title. American Mineralogist, in press.
DOI: https://doi.org/10.2138/am-2018-6058

Figure 7

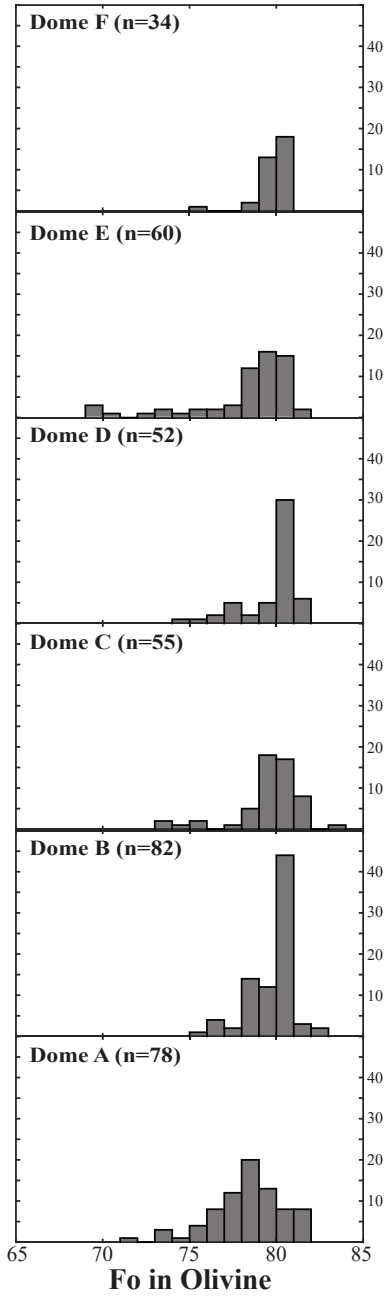

This is a preprint, the final version is subject to change, of the American Mineralogist (MSA)
Cite as Authors (Year) Title. American Mineralogist, in press.
DOI: https://doi.org/10.2138/am-2018-6058

Figure 8

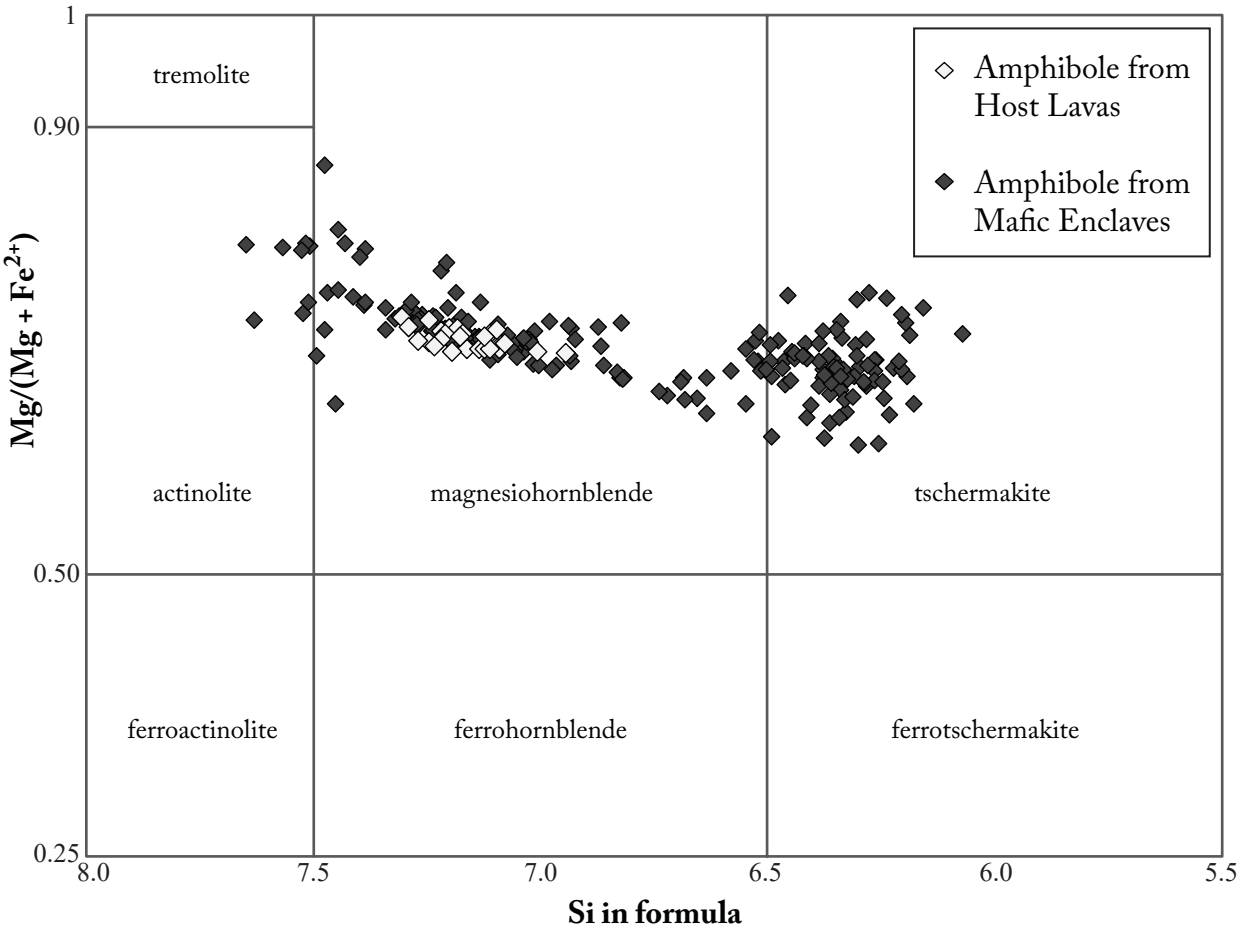

This is a preprint, the final version is subject to change, of the American Mineralogist (MSA)
Cite as Authors (Year) Title. American Mineralogist, in press.
DOI: https://doi.org/10.2138/am-2018-6058

Figure 9

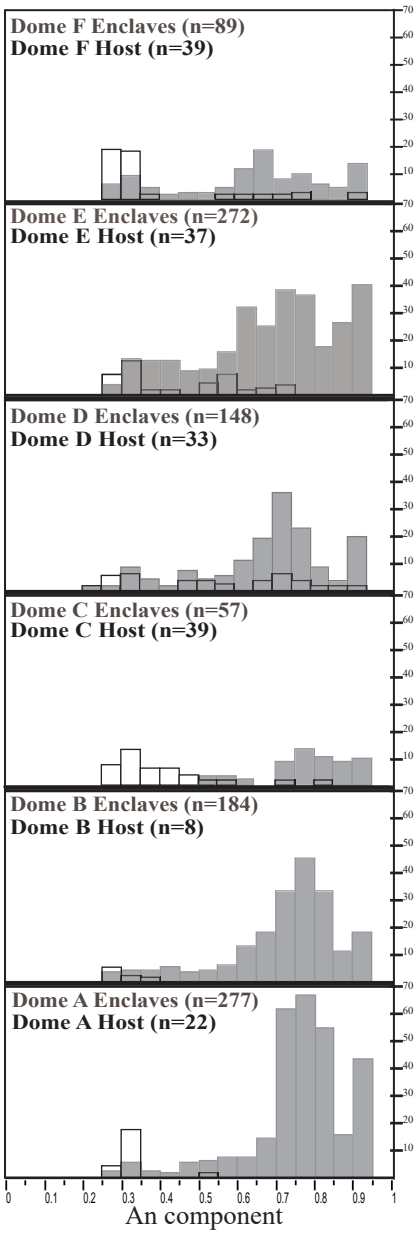

This is a preprint, the final version is subject to change, of the American Mineralogist (MSA)
Cite as Authors (Year) Title. American Mineralogist, in press.
DOI: https://doi.org/10.2138/am-2018-6058

Figure 10

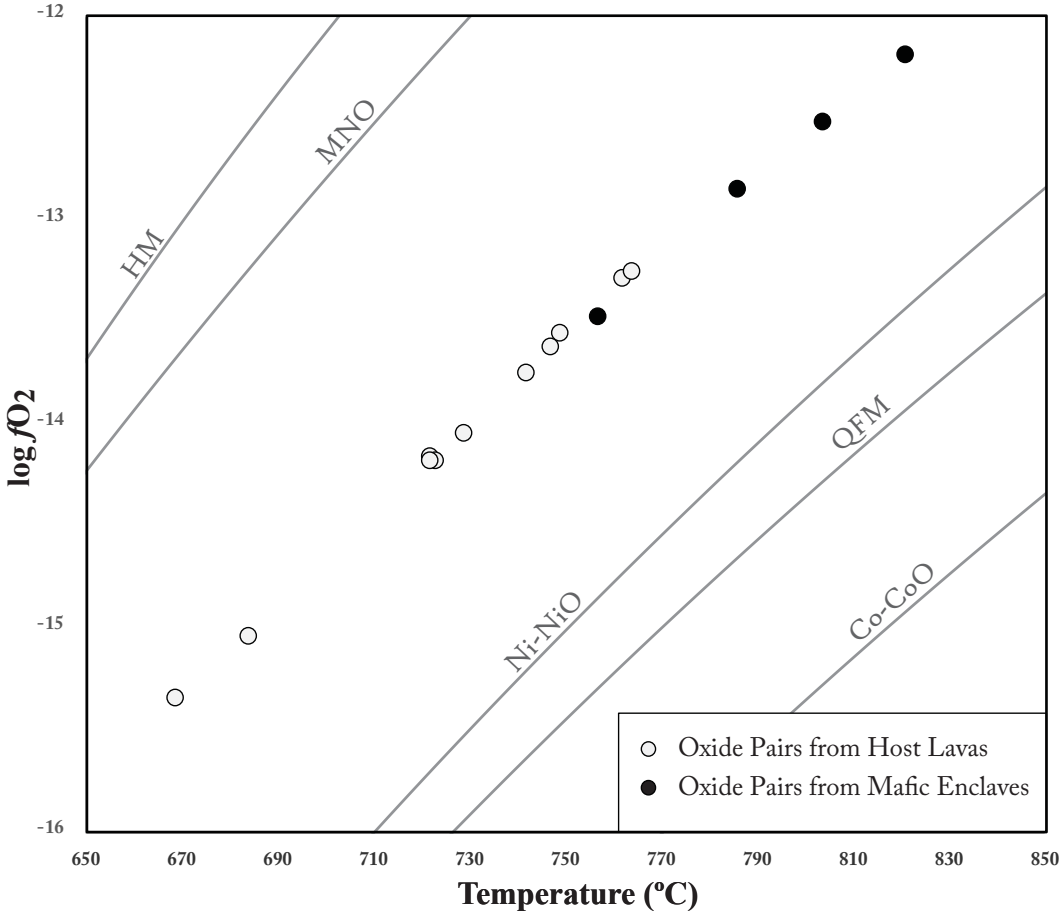

This is a preprint, the final version is subject to change, of the American Mineralogist (MSA)
Cite as Authors (Year) Title. American Mineralogist, in press.
DOI: https://doi.org/10.2138/am-2018-6058

Figure 11

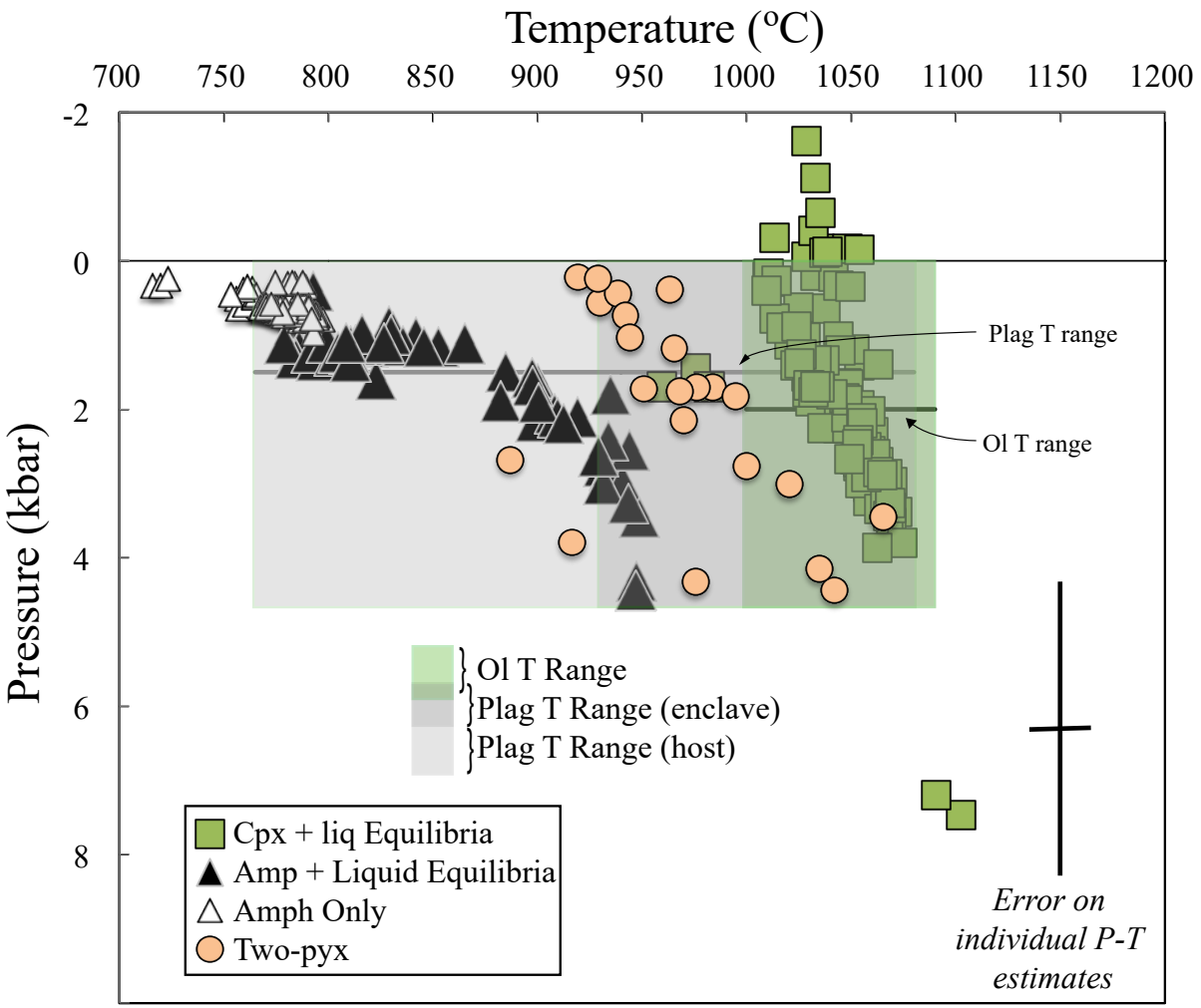

This is a preprint, the final version is subject to change, of the American Mineralogist (MSA)
Cite as Authors (Year) Title. American Mineralogist, in press.
DOI: https://doi.org/10.2138/am-2018-6058

Figure 12

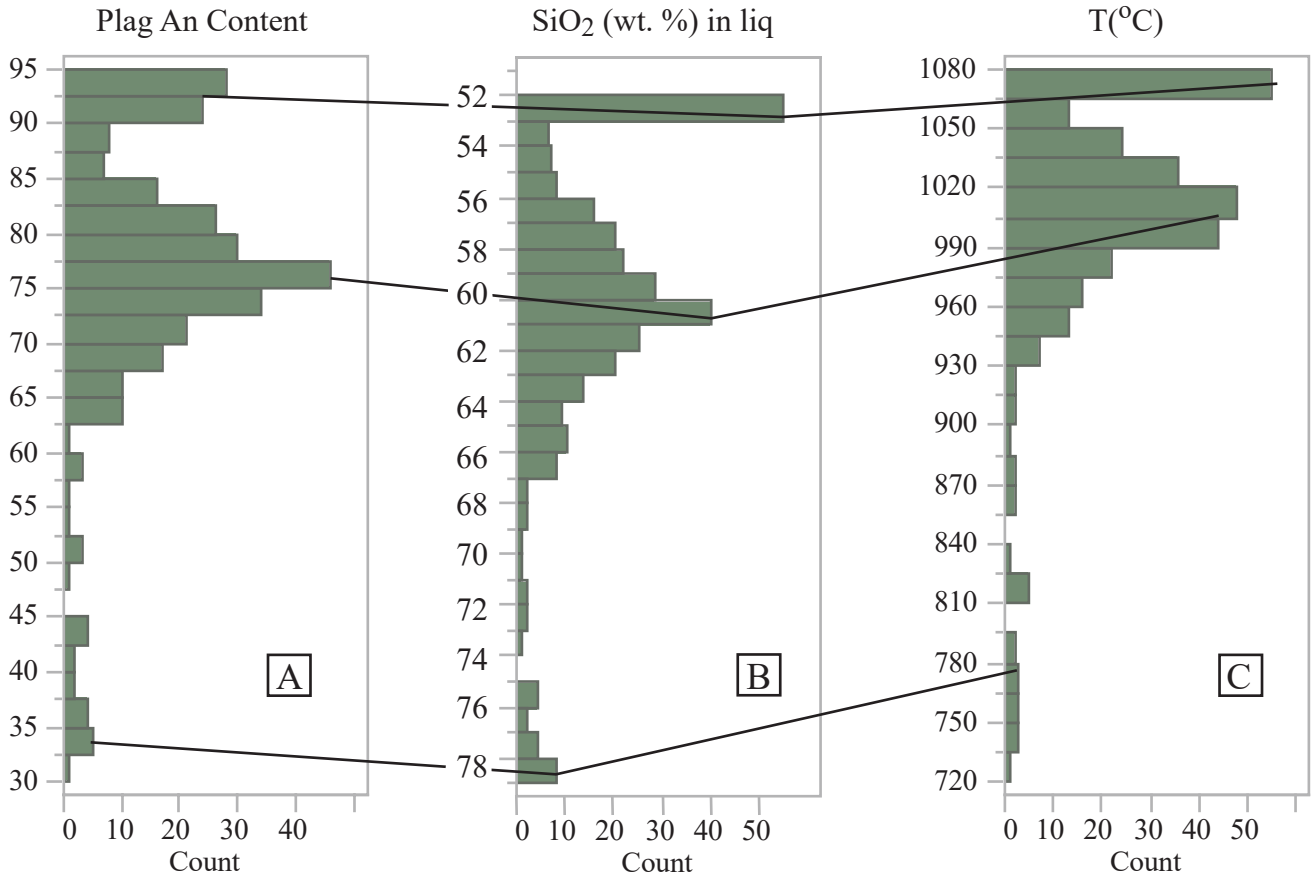

This is a preprint, the final version is subject to change, of the American Mineralogist (MSA)
Cite as Authors (Year) Title. American Mineralogist, in press.
DOI: https://doi.org/10.2138/am-2018-6058

Figure 13